Contrib Mineral Petrol (1981) 77:129–149

Contributions to Mineralogy and Petrology


# Chemical Evolution of a Pleistocene Rhyolitic Center: Sierra La Primavera, Jalisco, México

Gail A. Mahood
Department of Geology, School of Earth Sciences, Stanford University, Stanford, CA 94305, USA

**Abstract.** The late Pleistocene caldera complex of the Sierra La Primavera, Jalisco, México, contains well-exposed lava flows and domes, ash-flow tuff, air-fall pumice, and caldera-lake sediments. All eruptive units are high-silica rhyolites, but systematic chemical differences correlate with age and eruptive mode. The caldera-producing unit, the 45-km$^3$ Tala Tuff, is zoned from a mildly peralkaline first-erupted portion enriched in Na, Rb, Cs, Cl, F, Zn, Y, Zr, Hf, Ta, Nb, Sb, HREE, Pb, Th, and U to a metaluminous last-erupted part enriched in K, LREE, Sc, and Ti; Al, Ca, Mg, Mn, Fe, and Eu are constant within analytical errors. The earliest post-caldera lava, the south-central dome, is nearly identical to the last-erupted portion of the Tala Tuff, whereas the slightly younger north-central dome is chemically transitional from the south-central dome to later, more-mafic, ring domes. This sequence of ash-flow tuff and domes represents the tapping of progressively deeper levels of a zoned magma chamber 95,000 ± 5,000 years ago. Since that time, the lavas that erupted 75,000, 60,000, and 30,000 years ago have become decreasingly peralkaline and progressively enriched only in Si, Rb, Cs, and possibly U. They represent successive eruption of the uppermost magma in the post-95,000-year magma chamber.

Eruptive units of La Primavera are either aphyric or contain up to 15% phenocrysts of sodic sanidine ≧ quartz ≫ ferrohedenbergite > fayalite > ilmenite ± titanomagnetite. Whereas major-element compositions of sanidine, clinopyroxene, and fayalite phenocrysts changed only slightly between eruptive groups, concentrations of many trace elements changed by factors of 5 to 10, resulting in crystal/glass partition coefficients that differ by factors of up to 20 between successively erupted units. The extreme variations in partitioning behavior are attributed to small changes in bulk composition of the melt because major-element compositions of the phenocrysts and temperature, pressure, and oxygen fugacity of the magma all remained essentially constant.

Crystal settling and incremental partial melting by themselves appear incapable of producing either the chemical gradients within the Tala Tuff magma chamber or the trends with time in the post-caldera lavas. Transport of trace metals as volatile complexes within the thermal and gravitational gradient in volatile-rich but water-undersaturated magma is considered the dominant process responsible for compositional zonation in the Tala Tuff. The evolution of the post-caldera lavas with time is thought to involve the diffusive emigration of trace elements from a relatively dry magma as a decreasing proportion of network modifiers and/or a decreasing concentration of complexing ligands progressively reduced trace-metal-site availability in the silicate melt.

## Introduction

Studies of ash-flow tuffs, which are rapidly quenched voluminous samples of magma chambers, have led to characterization of the chemical and thermal gradients within the upper portions of silicic magma chambers just prior to eruption (Lipman et al. 1966; Smith and Bailey 1966; Hildreth 1977, 1979; Smith 1979; Ritchie 1980; Hildreth et al. 1980). Many ash flows show relatively small variations in major elements but extreme zonation in trace elements. The processes that produce this zoning are poorly understood, but a growing body of data (Shaw et al. 1976; Hildreth 1977, 1979; Smith 1979; Smith and MacDonald 1979) indicates that these chemical gradients cannot be explained by crystal settling in a high-level magma chamber or by crystal-liquid equilibrium during partial melting.

An ash-flow cooling unit is an inverted record of a magma chamber at a single point in time, whereas a sequence of eruptive units records the chemical evolution of a silicic magma chamber through time. If a lava flow or ash flow taps the most differentiated uppermost magma in the system at a particular moment, a sequence of eruptive units provides progress reports on the differentiation mechanisms operating at depth. The main purpose of this study of the Sierra La Primavera, therefore, has been to trace the chemical evolution of a rhyolitic complex through time, interpreting it as the periodic sampling of an evolving magma chamber.

The Sierra La Primavera, located on the western outskirts of Guadalajara, Jalisco, México (Fig. 1), was mapped at a scale of 1:25,000. Eruptive units were classified into groups based on stratigraphic relations, and the eruptive sequence was calibrated with over 50 K-Ar dates performed at University of California, Berkeley. This paper addresses the chemical evolution of the Primavera magma chamber as displayed in the compositions of ash-flow tuffs, lava flows, and domes erupted from it; the geologic evolution of the Sierra La Primavera is described elsewhere (Mahood 1980a, 1980b). A brief history of the Sierra follows and is summarized in Table 1.

## Summary of the Geologic History

The earliest lavas of the Sierra La Primavera erupted about 145,000 years ago. They were followed by eruption, approximately 95,000 years ago, of about 20 km$^3$ of magma as ash flows that formed the Tala Tuff. More than 90% of the volume of the tuff is aphyric; the last-erupted portion contains less than 1% sanidine and quartz. Collapse of the roof zone of the magma chamber upon eruption of the Tala Tuff produced an 11-km

0010-7999/81/0077/0129/$04.20

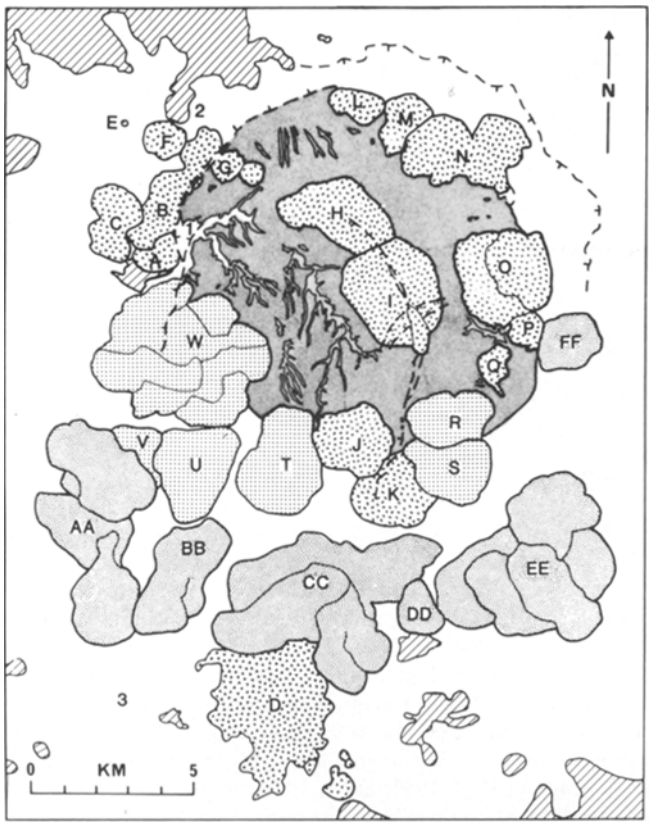


**Fig. 1.** Location map of the Sierra La Primavera. The Sierra La Primavera is located on the western outskirts of Guadalajara, Jalisco, México. *Diagonal ruling:* pre-Primavera volcanic rocks; *V-pattern:* pre-caldera lavas; *unpatterned:* Tala Tuff (also includes minor ash flows, primary and reworked air-fall deposits, and alluvium, all generally underlain by the Tala Tuff); *light stipple:* lake sediments; *double-dash pattern:* older ring domes; *rectilinear dots:* younger ring domes; *heavy stipple:* southern arc lavas. Faults are shown as *heavy dashed lines. Letters* refer to the names of eruptive centers as follows: *A* Río Salado dome; *B* Cañon de Las Flores flow: *C* Mesa El León dome; *D* Arroyo Saucillo group; *E* Mesa El Chiquihuitillo; *F* Mesa El Burro dome; *G* Cerro Chato dome; *H* Cerro Alto composite dome; *I* Mesa El Nejahuete composite dome; *J* Cerro El Tule dome; *K* El Madrón dome; *L* Pinar de La Venta dome; *M* Arroyo La Cuartilla dome; *N* Mesa La Lobera dome; *O* Cerro El Chapulín dome; *P* Dos Coyotes dome; *Q* Arroyo Las Pilas dome; *R* Arroyo Ixtahuatonte dome; *S* La Cuesta dome; *T* Cerro El Culebreado dome; *U* La Puerta dome; *V* Arroyo Las Animas dome; *W* Cerro El Pedernal center; *AA* Cerro San Miguel center; *BB* Llano Grande flow; *CC* Cerros Las Planillas center; *DD* Arroyo Colorado dome; *EE* Cerro El Tajo center; *FF* Cerro El Colli dome

diameter caldera that soon filled with water. The onset of lacustrine sedimentation was followed rapidly by eruption of two domes in the center of the lake (the south-central and north-central domes which form the lower portions of Mesa El Nejahuete and Cerro Alto, respectively, in Fig. 1). The base of the south-central dome occurs at the same position within the sediments as the "giant pumice horizon", an important stratigraphic marker. The north-central dome, however, overlies the giant pumice horizon. Ring domes representing some 5 $km^3$ of porphyritic magma then erupted along two concentric arcs: one along the northeast portion of the ring fracture and the other crossing the middle of the lake. A period of volcanic quiescence was marked by deposition of some 30 m of fine-grained ashy sediments. Activity resumed approximately 75,000 years ago with the eruption of 3 $km^3$ of aphyric and porphyritic magma at the southern margin of the lake, forming a younger group of ring domes. Ensuing uplift, thought to result from renewed insurgence of magma, brought an end to the lake. This uplift culminated in the eruption, beginning approximately 60,000 years ago, of 7 $km^3$ of aphyric lavas along a southern arc. The youngest of the southern arc lavas, Cerro El Colli, erupted approximately 25,000–30,000 years ago.

## Mineralogy

Phenocrysts in the porphyritic eruptive units range from less than 1% to 15% by volume. Sodic sanidine and quartz, the former generally more abundant, together comprise approximately 97–99% of the phenocrysts, the remainder being ferrohedenbergite, fayalite, and ilmenite, typically in the proportions 50:10:1. Rare titanomagnetite, zircon, and apatite are present in some units. Phenocryst assemblages of the various eruptive groups are summarized in Table 1.

The phenocryst assemblage found at La Primavera, with or without titanomagnetite, is common to many alkali rhyolites and mildly peralkaline comendites. It characterizes, for example, most of the silicic lavas of the Yellowstone plateau (R.L. Christiansen, personal communication, 1978), the first-erupted portion of the Bandelier Tuff, New Mexico (Smith and Bailey 1966), and a number of ash-flow tuffs in Nevada, including the Grouse Canyon Member of the Belted Range Tuff (Noble et al. 1969), the Spearhead Member of the Thirsty Canyon Tuff (Noble and Parker 1974), and the Kane Springs Wash Tuff (Noble 1968). It also is the phenocrystic assemblage of some hypersolvus granites [e.g., the Liruei complex of northern Nigeria (Jacobsen et al. 1958)]. Where the compositions of phenocrysts have been determined, they are generally similar to those of La Primavera. The alkali feldspar is a sodic sanidine rather than the true anorthoclase found in more strongly peralkaline rocks. The olivine and clinopyroxene are exceedingly iron-rich, often containing more manganese than magnesium, and the clinopyroxene is a ferrohedenbergite with only moderate amounts of sodium.

Phenocrysts from 25 samples were analyzed with the electron microprobe. Analyses of representative samples appear in Tables 2 through 5; the remainder of the analyses may be obtained by writing the author. Sanidine, ferrohedenbergite, and ilmenite are unzoned and homogeneous. The range of analyses within a sample is only slightly greater than that found within a single grain, and much of the latter can be attributed to electron-microprobe counting statistics. The compositions of the phenocrysts changed slightly with time, but within eruptive groups the phenocrysts are uniform in composition.

### *Quartz*

Quartz phenocrysts are generally resorbed and embayed, resulting in nearly spherical grains 0.3 to 2.0 mm in diameter. In some samples the quartz retains its original bipyramidal shape. Glass inclusions are common.

### *Sanidine*

Sodic sanidine occurs as clear, simply twinned, tabular grains 0.5–2.5 mm in length. Rarely it has tiny inclusions of ferrohedenbergite or fayalite. Iron, expressed as $Fe_2O_3$, is present at slightly more than 0.2 wt.% in all age groups (Table 2). CaO ranges from 0.04 to 0.15% with a tendency for the younger ring domes to have the lower values. Sanidine in the pre-caldera lavas and younger ring domes is more potassic than sanidine from the last-erupted Tala Tuff, the south-central dome, the giant pumice horizon, and the older ring domes (Fig. 2). The most sodic sanidine occurs in the north-central dome.

**Table 1.** Summary of the geologic history of the Sierra La Primavera

| Event | Approximate age in years based on K–Ar dates (Mahood 1980a) | Magma volume ($km^3$) | % total phenocrysts | Phenocryst assemblage |
|---|---|---|---|---|
| Eruption of pre-caldera lavas | 144,000–100,000 | 2(?) | 0 or 10–15 | San ≧ Q ≫ Cpx ≫ Fa > Ilm > Mt |
| Eruption of the Tala Tuff | | 20 | 0–1 | San ≧ Q |
| Caldera collapse | | | | |
| Eruption of central domes and deposition of giant pumice horizon | 95,000 ± 10,0000 | | | |
| Giant pumice horizon | | 0.15 | 1 | San > Q ≫ Cpx ≫ Ilm |
| South-central dome | | 0.8 | 1 | San > Q ≫ Cpx > Fa ≫ Ilm |
| North-central dome | | 0.7 | 10 | San > Q ≫ Cpx > Fa ≫ Ilm |
| Eruption of older ring domes | | 5 | 10–15 | San ≧ Q ≫ Cpx > Fa ≫ Ilm |
| Eruption of younger ring domes | 75,000 | 3 | 0 or 10 | San ≧ Q ≫ Cpx > Fa ≫ Ilm |
| Uplift | | | | |
| Eruption of southern arc lavas | 60,000 and 30,000 | 7 | 0 | None |

**Table 2.** Microprobe analyses of sanidine[a]

| | Pre-caldera domes | | Tala Tuff | | Central domes and giant pumice horizon | | | Older ring domes | | | | Younger ring domes | |
|---|---|---|---|---|---|---|---|---|---|---|---|---|---|
| Sample number | 193 | 186 | 252 | 218 | 317 | 283 | 234 | 89 | 92 | 133 | 37 | 79 | 174 |
| Eruptive unit[a] | A | C | 1 | 1 | I | H | gph | F | G | J | M | R | W |
| $SiO_2$ | 66.0 | 66.3 | 66.9 | 66.6 | 66.7 | 67.0 | 67.1 | 66.4 | 66.3 | 66.9 | 66.5 | 66.2 | 66.4 |
| $Al_2O_3$ | 19.5 | 19.0 | 19.5 | 19.3 | 19.4 | 19.4 | 19.6 | 19.2 | 19.1 | 19.1 | 19.3 | 18.7 | 19.0 |
| $Fe_2O_3$ | 0.22 | 0.24 | 0.20 | 0.21 | 0.22 | 0.21 | 0.22 | 0.24 | 0.22 | 0.22 | 0.23 | 0.24 | 0.26 |
| CaO | 0.08 | 0.10 | 0.15 | 0.14 | 0.13 | 0.13 | 0.11 | 0.10 | 0.08 | 0.12 | 0.11 | 0.05 | 0.04 |
| $Na_2O$ | 6.17 | 6.08 | 6.71 | 6.68 | 6.67 | 6.98 | 6.81 | 6.81 | 6.75 | 6.74 | 6.68 | 6.26 | 6.45 |
| $K_2O$ | 7.94 | 7.95 | 7.32 | 7.21 | 7.29 | 6.97 | 7.10 | 7.17 | 7.19 | 7.01 | 7.16 | 7.63 | 7.69 |
| BaO | – | 0.06 | – | – | – | – | – | 0.01 | 0.02 | 0.07 | 0.05 | 0.04 | 0.01 |
| Total | 99.9 | 99.8 | 100.7 | 100.1 | 100.4 | 100.7 | 100.9 | 100.0 | 99.6 | 100.2 | 100.0 | 99.1 | 99.8 |
| Analyses recalculated to mole percent feldspar molecules | | | | | | | | | | | | | |
| Or | 47.1 | 47.5 | 42.9 | 42.7 | 43.0 | 40.8 | 41.9 | 42.2 | 42.5 | 41.8 | 42.6 | 45.9 | 45.3 |
| Ab | 52.5 | 52.0 | 56.3 | 56.6 | 56.4 | 58.5 | 57.6 | 57.3 | 57.1 | 57.6 | 56.9 | 53.9 | 54.5 |
| An | 0.4 | 0.5 | 0.7 | 0.7 | 0.6 | 0.6 | 0.5 | 0.5 | 0.4 | 0.4 | 0.5 | 0.3 | 0.2 |
| Total apparent compositional range within sample | | | | | | | | | | | | | |
| Or | 3.8 | 3.8 | 3.6 | 5.1 | 4.4 | 6.7 | 5.4 | 6.0 | 3.8 | 2.1 | 7.5 | 4.0 | 3.8 |
| Ab | 3.2 | 3.4 | 4.1 | 2.8 | 5.5 | 7.4 | 5.5 | 6.1 | 5.3 | 3.8 | 5.7 | 5.6 | 4.5 |
| An | 0.4 | 0.4 | 0.5 | 0.5 | 0.4 | 0.5 | 0.5 | 0.7 | 0.5 | 0.4 | 0.9 | 0.4 | 0.2 |

[a] Eruptive unit letters are keyed to Fig. 1, except for gph, which refers to the giant pumice horizon

*Ferrohedenbergite*

Ferrohedenbergite is the most abundant ferromagnesian phase. It occurs as slightly pleochroic, green to brownish-green, prismatic grains 0.7–1.2 mm long, and commonly contains ilmenite inclusions. Alumina is fairly uniform at slightly more than 0.2 wt.% in all samples (Table 3). The south-central dome has the most Fe-rich and Mg-poor ferrohedenbergite, whereas the pyroxenes of the giant pumice horizon and north-central dome are the richest in Mg and Mn. Mg and Mn then decreased progressively in the older and younger ring domes (Fig. 2). The ferrohedenbergite of the pre-caldera lavas and younger ring domes is slightly richer in Na and Ca but is poorer in Ti.

*Fayalite*

Fayalite occurs as small, round, honey-colored grains, few larger than 0.2 mm in diameter. Most grains contain ilmenite inclusions and are rimmed by opaque alteration products. Most samples contain two populations of fayalite (Table 4): one apparently normal in composition and the other giving consistently low microprobe totals. The deficiencies result from apparent decreases in FeO* (total iron as FeO) and MnO of approximately 7% and 0.4%, respectively, that are only partially compensated by increases of 2% in $SiO_2$ and 0.1% in $Al_2O_3$.

Fe-deficient fayalite occurs both as dark-colored, nearly opaque rims on normal fayalite and as small separate grains. The fayalites

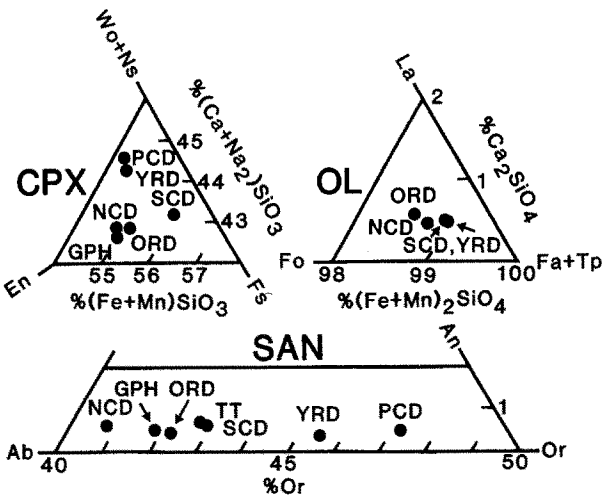


**Fig. 2.** Plot of sodic sanidine, ferrohedenbergite, and fayalite compositions. *TT* Tala Tuff; *SCD* south-central dome; *GPH* giant pumice horizon; *NCD* north-central dome; *ORD* older (95,000-year) ring domes; *YRD* younger (75,000-year) ring domes. Phenocryst compositions do not vary regularly with position in the eruptive sequence

were also analyzed for Na, Ni, Zr, and $O_2$ to see if these elements might account for the deficiency. Ni, Zr, and Na were not detected. The oxygen analyses, although not quantitative, show a significant increase in the iron-poor rims, which suggests that iron is present in the $Fe^{+3}$ oxidation state and/or that the rims are hydrated. It is noteworthy that the only two samples in which fayalite is entirely the Fe-deficient type are the pre-caldera lavas that contain titanomagnetite. This suggests that the Fe-deficient fayalite is an oxidation product of normal fayalite, produced when conditions moved from the fayalite stability field (below the FMQ buffer) to where quartz and magnetite are stable, due to an increase in $f_{O_2}$ and/or decrease in temperature. Both conditions are likely as magma moves toward the surface just prior to eruption.

Chemical variation in normal fayalite among the eruptive groups is small (Table 4). As is the case for ferrohedenbergite, Mg and Ca are lower in fayalite from the pre-caldera lavas, the younger ring domes and the south-central dome than from the older ring domes and north-central dome (Fig. 2).

*Ilmenite*

Homogeneous ilmenite occurs as tiny plate-like inclusions in ferrohedenbergite and fayalite, and less commonly as separate phenocrysts approximately 0.2 mm in diameter. Included ilmenite has the same composition as separate phenocrysts. Values for $Al_2O_3$, MgO, and CaO are consistently less than 0.1 wt.% and are approximately constant in phenocrysts of all age groups (Table 5). Values for MnO and the Ti/Fe ratio fall into two groups: lower values in the pre-caldera lavas, the south-central domes and younger ring domes, and higher values in the giant pumice horizon, the north-central dome, and older ring domes.

*Titanomagnetite*

Only pre-caldera lavas contain titanomagnetite. In the Mesa El León flow, it is oxidized/exsolved, but in the Río Salado flow titanomagnetite is homogeneous and of one population, the composition of which is listed in Table 5. The titanomagnetite in these units also contains zircon inclusions, which are exceedingly rare in other species and units of La Primavera.

**Table 3.** Microprobe analyses of ferrohedenbergite

| | Pre-caldera domes | | Central domes and giant pumice horizon | | | Older ring domes | | | | Younger ring domes | |
|---|---|---|---|---|---|---|---|---|---|---|---|
| Sample number | 193 | 186 | 317 | 283 | 234 | 89 | 92 | 133 | 37 | 79 | 174 |
| Eruptive unit | A | C | I | H | gph | F | G | J | M | R | W |
| $SiO_2$ | 47.5 | 48.1 | 47.3 | 47.6 | 47.8 | 48.4 | 47.9 | 48.0 | 48.1 | 48.1 | 48.0 |
| $TiO_2$ | 0.19 | 0.21 | 0.28 | 0.33 | 0.31 | 0.33 | 0.31 | 0.31 | 0.33 | 0.23 | 0.24 |
| $Al_2O_3$ | 0.25 | 0.23 | 0.29 | 0.24 | 0.24 | 0.26 | 0.22 | 0.25 | 0.22 | 0.22 | 0.21 |
| FeO* | 30.3 | 29.6 | 31.0 | 30.3 | 30.3 | 30.1 | 30.1 | 29.9 | 30.1 | 29.9 | 30.0 |
| MnO | 1.37 | 1.34 | 1.36 | 1.54 | 1.56 | 1.52 | 1.46 | 1.49 | 1.51 | 1.39 | 1.35 |
| MgO | 0.34 | 0.43 | 0.28 | 0.71 | 0.75 | 0.62 | 0.61 | 0.59 | 0.62 | 0.44 | 0.40 |
| CaO | 18.9 | 18.8 | 18.5 | 18.5 | 18.4 | 18.4 | 18.4 | 18.5 | 18.5 | 18.7 | 18.7 |
| $Na_2O$ | 0.72 | 0.64 | 0.56 | 0.50 | 0.48 | 0.52 | 0.54 | 0.53 | 0.52 | 0.65 | 0.66 |
| Total | 99.6 | 99.6 | 99.5 | 99.8 | 99.9 | 100.0 | 99.6 | 99.5 | 99.9 | 99.6 | 99.5 |
| Formulae calculated on basis of 6 oxygens ($XYZ_2O_6$) | | | | | | | | | | | |
| Z: Si | 1.98 | 2.00 | 1.98 | 1.98 | 1.98 | 2.00 | 1.99 | 1.99 | 1.99 | 2.00 | 2.00 |
| Al | 0.012 | – | 0.014 | 0.012 | 0.012 | 0.002 | 0.008 | 0.005 | 0.006 | 0.004 | 0.004 |
| XY: Ca | 0.846 | 0.839 | 0.829 | 0.826 | 0.821 | 0.812 | 0.821 | 0.824 | 0.821 | 0.835 | 0.833 |
| Na | 0.058 | 0.051 | 0.045 | 0.040 | 0.038 | 0.042 | 0.043 | 0.043 | 0.042 | 0.052 | 0.053 |
| Fe | 1.06 | 1.03 | 1.08 | 1.05 | 1.05 | 1.04 | 1.05 | 1.04 | 1.04 | 1.04 | 1.04 |
| Mn | 0.048 | 0.047 | 0.048 | 0.054 | 0.055 | 0.053 | 0.051 | 0.052 | 0.053 | 0.049 | 0.048 |
| Mg | 0.021 | 0.027 | 0.017 | 0.044 | 0.046 | 0.038 | 0.038 | 0.036 | 0.038 | 0.027 | 0.025 |
| Ti | 0.006 | 0.007 | 0.009 | 0.010 | 0.010 | 0.010 | 0.010 | 0.010 | 0.010 | 0.007 | 0.008 |
| Al | – | 0.011 | – | – | – | 0.011 | 0.003 | 0.007 | 0.005 | 0.007 | 0.006 |
| Total Z: | 2.00 | 2.00 | 1.99 | 1.99 | 2.00 | 2.00 | 2.00 | 2.00 | 2.00 | 2.00 | 2.00 |
| Total XY: | 2.04 | 2.01 | 2.03 | 2.03 | 2.02 | 2.01 | 2.01 | 2.01 | 2.01 | 2.02 | 2.02 |

The averages of the total apparent ranges of oxide analyses within a sample in wt.% follow: $SiO_2$, 1.3; $TiO_2$, 0.13; $Al_2O_3$, 0.20; FeO*, 1.2; MnO, 0.30; MgO, 0.47; CaO, 1.1; $Na_2O$, 0.18. Some of the variation is due to microprobe error; therefore, these values are maxima for the real variations

**Table 4.** Microprobe analyses of fayalite

| | Pre-caldera domes | | Central domes | | Older ring domes | | | | | Younger ring domes | |
|---|---|---|---|---|---|---|---|---|---|---|---|
| Sample number | 193 | 186 | 317 | 283 | 89 | 89[a] | 92 | 133 | 37 | 79 | 174 |
| Eruptive unit | A | C | I | H | F | F | G | J | M | R | W |
| $SiO_2$ | 32.5 | 33.6 | 29.5 | 29.4 | 30.4 | 32.4 | 30.7 | 30.1 | 29.9 | 30.2 | 30.6 |
| $TiO_2$ | 0.01 | 0.03 | 0.02 | 0.02 | 0.05 | 0.06 | 0.03 | 0.03 | 0.03 | 0.03 | 0.02 |
| $Al_2O_3$ | 0.10 | 0.18 | 0.02 | 0.04 | 0.03 | 0.18 | 0.05 | 0.04 | 0.02 | 0.02 | 0.04 |
| FeO* | 56.4 | 56.5 | 64.8 | 64.7 | 65.2 | 58.4 | 65.4 | 64.7 | 64.5 | 65.7 | 64.9 |
| MnO | 3.41 | 3.48 | 3.45 | 3.64 | 3.66 | 3.31 | 3.73 | 3.76 | 3.71 | 3.55 | 3.79 |
| MgO | 0.15 | 0.15 | 0.19 | 0.28 | 0.28 | 0.24 | 0.29 | 0.38 | 0.33 | 0.19 | 0.20 |
| CaO | 0.19 | 0.22 | 0.27 | 0.28 | 0.31 | 0.29 | 0.31 | 0.30 | 0.28 | 0.25 | 0.23 |
| ZnO | 0.06 | 0.06 | 0.13 | 0.08 | – | – | – | 0.11 | 0.10 | 0.12 | 0.16 |
| Total | 92.8 | 94.2 | 98.4 | 98.4 | 100.0 | 94.9 | 100.5 | 100.5 | 98.8 | 100.0 | 100.0 |
| Formulae recalculated to mole percent olivine molecules | | | | | | | | | | | |
| Fa | | | 93.9 | 93.5 | 93.4 | | 93.3 | 93.0 | 93.2 | 93.9 | 93.5 |
| Tp | | | 5.1 | 5.3 | 5.3 | | 5.4 | 5.4 | 5.4 | 5.1 | 5.5 |
| Fo | All Fe-deficient | | 0.5 | 0.7 | 0.7 | Fe-deficient | 0.7 | 1.0 | 0.9 | 0.5 | 0.5 |
| La | | | 0.5 | 0.5 | 0.6 | | 0.6 | 0.6 | 0.5 | 0.5 | 0.4 |

[a] Fe-deficient fayalite within Sample 89

**Table 5.** Microprobe analyses of ilmenite and titanomagnetite

| | Ilmenite | | | | | | | | | | | Titanomagnetite |
|---|---|---|---|---|---|---|---|---|---|---|---|---|
| | Pre-caldera domes | | Central domes and giant pumice horizon | | | Older ring domes | | | | Younger ring domes | | Pre-caldera dome |
| Sample number | 193 | 186 | 317 | 283 | 234 | 89 | 92 | 133 | 37 | 79 | 174 | 193 |
| Eruptive unit | A | C | I | H | gph | F | G | J | M | R | W | A |
| $SiO_2$ | 0.00 | 0.32 | 0.02 | 0.05 | 0.00 | 0.37 | 0.27 | 0.26 | 0.16 | 0.10 | 0.30 | 0.03 |
| $TiO_2$ | 49.2 | 48.4 | 49.6 | 50.3 | 50.5 | 48.2 | 49.7 | 49.6 | 49.7 | 49.5 | 48.9 | 16.8 |
| $Al_2O_3$ | 0.00 | 0.05 | 0.04 | 0.06 | 0.02 | 0.05 | 0.06 | 0.02 | 0.00 | 0.00 | 0.06 | 0.26 |
| FeO* | 48.4 | 47.1 | 47.9 | 47.1 | 47.1 | 46.9 | 45.8 | 47.3 | 46.8 | 47.6 | 47.3 | 76.5 |
| MnO | 1.34 | 1.37 | 1.27 | 1.44 | 1.38 | 1.44 | 1.42 | 1.47 | 1.39 | 1.33 | 1.33 | 0.81 |
| MgO | 0.04 | 0.07 | 0.04 | 0.06 | 0.06 | 0.06 | 0.05 | 0.07 | 0.06 | 0.04 | 0.04 | 0.03 |
| CaO | 0.02 | 0.02 | 0.02 | 0.03 | 0.02 | 0.03 | 0.03 | 0.02 | 0.02 | 0.04 | 0.07 | 0.01 |
| ZnO | 0.10 | 0.09 | 0.09 | 0.09 | 0.06 | 0.14 | 0.05 | 0.06 | 0.05 | 0.08 | 0.07 | 0.33 |
| Total | 99.1 | 97.4 | 99.0 | 99.1 | 99.1 | 97.2 | 97.4 | 98.8 | 98.2 | 98.7 | 98.0 | 94.7 |
| Analyses recalculated following Carmichael (1967) | | | | | | | | | | | | |
| $Fe_2O_3$ | 6.23 | 5.40 | 5.35 | 3.94 | 3.66 | 5.46 | 2.64 | 4.46 | 3.86 | 5.06 | 5.08 | 35.0 |
| FeO | 42.7 | 42.2 | 43.1 | 43.6 | 43.8 | 42.0 | 43.4 | 43.2 | 43.3 | 43.1 | 42.7 | 45.0 |
| New total | 99.7 | 97.9 | 99.5 | 99.5 | 99.5 | 97.7 | 97.7 | 99.2 | 98.6 | 99.2 | 98.5 | 98.2 |
| Mole % $R_2O_3$ | 5.95 | 5.32 | 5.18 | 3.86 | 3.53 | 5.44 | 2.65 | 4.30 | 3.73 | 4.86 | 4.99 | % Usp. 48.6 |

## Intensive Parameters

### *Temperature and Oxygen Fugacity*

Neither the aphyric nature of many Primavera eruptive units nor the phenocryst assemblages in most others lend themselves to thermodynamic determination of crystal-liquid equilibration temperatures. Hence it remains uncertain whether the chemical evolution documented for the post-caldera lavas took place under a waxing, waning, or fluctuating thermal regime.

Microprobe analyses of titanomagnetite and ilmenite from the Río Salado dome were recalculated (Carmichael 1967), and the recast analyses were used to determine the temperature and oxygen fugacity (Buddington and Lindsley 1964). A temperature of 850° C and a $\log f_{O_2}$ of −13.8 were obtained, which are appropriate to a magma on the FMQ buffer. The temperature is similar to the 885° C obtained by the author for a high-silica rhyolite from the Yellowstone Plateau that bears a mineral assemblage identical to La Primavera and is also in agreement with the range of 790°–925° C found by Carmichael (1967) for fayalite-bearing rhyolites.

The lack of titanomagnetite in any of the other fayalite-bearing lavas suggests that these magmas equilibrated slightly below the FMQ buffer. The small variations between eruptive units of the major-element compositions of phenocrysts suggest only small differences in magma temperatures and $f_{O_2}$. This fact, coupled with the results of a geothermometer based on partitioning of the $Fe_2SiO_4$ component

between olivine and the liquid (Ghiorso and Carmichael 1980) and a geothermometer based on the exchange reaction of FeO and MnO between ilmenite and olivine (Mahood 1980a), results in the conclusion that eruptive temperatures of porphyritic Primavera magmas probably varied by no more than 30° C. The aphyric nature of the southern arc magmas requires that either they were slightly hotter than the other Primavera lavas or they contained more dissolved volatiles which lowered the liquidus temperature.

### *Total Pressure*

*Geological Constraints.* Formation of a caldera 11 km in diameter on eruption of only 20 $km^3$ of magma as the Tala Tuff would seem to require a magma chamber with a fairly shallow roof. If the magma had erupted from great depth, compensation at the surface for this small volume would have been minimal and probably would have occurred along regional lines of weakness rather than as a nearly perfectly circular caldera. By analogy with eroded cauldrons and ring complexes of similar mineralogy and bulk composition, the roof of the Primavera magma chamber was probably between 2 and 6 km beneath the surface. Assuming that the phenocrysts precipitated near the roof zone of a high-level magma chamber, the small variation between eruptive groups of the major-element compositions of the phenocrysts suggests that the depth to the roof of this magma chamber changed little after eruption of the Tala Tuff.

*Calculated Pressure.* The pressure estimated from such geological evidence (1 to 2 kb) is smaller than the equilibration pressure calculated by the method of Nicholls et al. (1971) for the Río Salado dome using the following reaction:

$$3Fe_2SiO_4 + O_2 = 2Fe_3O_4 + 3SiO_2.$$
$$\text{(fayalite)} + \text{(gas)} = \text{(magnetite)} + \text{(quartz)}$$

All the fayalite of the Río Salado flow is deficient in iron due to late-stage alteration. This in itself indicates that the fayalite was not in equilibrium with the melt at eruption and, therefore, the Fe-Ti-oxide temperature and oxygen fugacity may not apply to the fayalite. The pressure calculated using a hypothetical alteration-free fayalite is $3.4 \pm 2$ kbars, equivalent to a depth of approximately $11 \pm -7$ km.

Depths of 11 km or more *may* be reasonable for the pre-caldera lavas, whose vent patterns and erratic chemical variations with time suggest that they may have erupted prior to the development of a well-integrated magma chamber at La Primavera. If so, phenocryst compositions may reflect conditions at the source or some intermediate level. However, phenocryst compositions in the pre-caldera lavas are similar to those of the younger ring domes, for which, like the older ring domes, there is good evidence for eruption from a high-level magma chamber along a ring-fracture zone.

### *Water Fugacity*

Lack of a hydrous phase in La Primavera rocks does not necessarily indicate that the water fugacity was extremely low. Primavera magmas probably had temperatures close to 850° C and were, therefore, near the upper stability limit of hydrous biotite, which at this temperature has an Mg/Fe ratio of about 0.5 (Wones and Eugster 1965). Comparison with the $(Mg/Fe_{biotite})/(Mg/Fe_{rock})$ ratio over the temperature range of the Bishop Tuff (Hildreth 1977) shows that Primavera magmas have whole-rock Mg/Fe ratios much too small to produce a hydrous biotite stable at 850° C. At low water concentrations, biotite appears at low temperatures late in the crystallization sequence, following quartz and alkali feldspar (Maaløe and Wyllie 1975; Naney and Swanson 1980). Similarly, alkali amphiboles are commonly restricted to the groundmass of volcanic peralkaline rocks, suggesting that they are stable only at lower temperatures. It appears that Primavera magmas were too hot and/or too low in bulk Mg/Fe ratio to precipitate biotite or amphibole.

## Whole-Rock Chemistry

Nearly all the eruptive units of the Sierra La Primavera are mildly peralkaline high-silica rhyolites (>75 wt.% $SiO_2$ on an anhydrous basis). Although all units are similar in gross composition, there are systematic chemical differences that correlate with both their age and eruptive mode. Variations in major-element compositions at La Primavera are small; in contrast, variations in the minor and trace elements are striking.

Preliminary XRF scans for Rb, Sr, Y, Zr, and Nb on over 150 samples of lavas, ash flows, and air-fall tephra from La Primavera, as well as electron microprobe analyses of phenocrysts and wet-chemical analyses of some samples, established that (1) the pre-caldera lavas are not identical; (2) the Tala Tuff is mildly compositionally zoned; (3) Cerro Alto and Mesa El Nejahuete are composite domes formed by eruption of lavas of different compositions; (4) the older (95,000-year) ring domes are chemically homogeneous and virtually identical to one another; (5) the compositions of the younger (75,000-year) ring domes vary only slightly; (6) the southern arc lavas are homogeneous and identical to one another with the exception of Cerro El Colli, which is chemically distinct. On the basis of these exploratory analyses, 29 samples of lavas from the various eruptive groups and pumice from the Tala Tuff were selected for precise quantitative analyses of major and minor elements by classical wet chemistry (Table 6), and of minor and trace elements by instrumental neutron activation analysis (INAA) and X-ray fluorescence (XRF) (Table 7). Wet-chemical, INAA, and XRF analyses of additional samples may be obtained by writing the author. Sample descriptions and localities for the representative samples are found in Appendix 1.

Pumiceous rocks and pumice lapilli from the Tala Tuff have been hydrated to a significant degree and, as a result, have approximately 0.3 wt.% less $Na_2O$, 0.2 wt.% more $K_2O$, and higher $Fe_2O_3/FeO$ ratios than do dense obsidians (otherwise chemically identical) from corresponding eruptive groups (e.g., pumiceous Sample 174 versus obsidian Sample 175). For this reason, the agpaitic index (molar ratio $(Na_2O+K_2O)/Al_2O_3$) calculated from an analysis may only approximate the magmatic value, which, if different, is likely to have been slightly higher. Elements such as Zr and Hf that invariably increase with increasing peralkalinity within a comagmatic suite (Macdonald and Bailey 1973; Watson 1979) are probably better indicators of the original peralkalinity of the magma. Perlitic but non-pumiceous samples (e.g., most of the older ring domes) are affected to a lesser degree. The consistent values for $Na_2O$ and $K_2O$ for all the 60,000-year southern arc lavas indicate that these obsidians have been modified very little. In the following discussion, samples with variable degrees of post-eruptive hydration are compared on the basis of analyses recalculated free of water and normalized to 100%.

### *Pre-Caldera Lavas*

The pre-caldera lavas are the most heterogenous eruptive group (Tables 6 and 7). The three units for which relative ages are known (in order of descending age, Samples 193, 90, and 186) show no systematic chemical trends with time.

### *Tala Tuff*

The Tala Tuff is weakly compositionally zoned from a mildly peralkaline first-erupted portion (agpaitic index=1.10, Zr≈ 600 ppm) to a barely metaluminous last-erupted part (agpaitic

**Table 6.** Wet-chemical major element analyses[a]

| | Pre-caldera lavas | | | | Tala Tuff | | | | | | | Central domes and giant pumice horizon | | |
|---|---|---|---|---|---|---|---|---|---|---|---|---|---|---|
| Sample number[b] | 290 | 193 | 90 | 186 | 323 | 184 | 255 | 256 | 210 | 252 | 218 | 317 | 234 | 283 |
| Eruptive unit[c] | D | A | B | C | e | e | e | m | m | l | l | I | gph | H |
| Porphyritic (p) or aphyric (a) | a | p | a | p | a | a | a | a | a | p | p | p | p | p |
| $SiO_2$ | 76.02 | 74.37 | 75.23 | 73.92 | – | 74.01 | – | – | – | 74.16 | 74.33 | 76.00 | 73.76 | 74.64 |
| $TiO_2$ | 0.12 | 0.09 | 0.15 | 0.11 | 0.08 | 0.09 | 0.08 | 0.12 | 0.10 | 0.13 | 0.13 | 0.13 | 0.16 | 0.18 |
| $Al_2O_3$ | 11.32 | 11.41 | 12.05 | 11.70 | 11.40 | 11.33 | 11.45 | 11.83 | 11.36 | 11.53 | 11.29 | 11.57 | 11.33 | 11.39 |
| $Fe_2O_3$ | 0.73 | 0.82 | 0.71 | 1.26 | 1.23 | 1.10 | 1.23 | 1.33 | 1.71 | 1.12 | 1.59 | 0.74 | 0.79 | 0.72 |
| FeO | 1.02 | 0.76 | 1.29 | 0.43 | 0.53 | 0.65 | 0.54 | 0.53 | 0.01 | 0.59 | 0.23 | 1.08 | 1.01 | 1.02 |
| MnO | 0.04 | 0.04 | 0.06 | 0.04 | 0.04 | 0.05 | 0.04 | 0.04 | 0.02 | 0.04 | 0.05 | 0.05 | 0.05 | 0.05 |
| MgO | 0.04 | 0.05 | 0.06 | 0.04 | – | 0.04 | 0.04 | 0.04 | 0.02 | 0.04 | 0.05 | 0.05 | 0.05 | 0.05 |
| CaO | 0.22 | 0.20 | 0.34 | 0.25 | 0.14 | 0.17 | 0.14 | 0.18 | 0.18 | 0.16 | 0.25 | 0.27 | 0.22 | 0.20 |
| $Na_2O$ | 4.62 | 4.11 | 4.76 | 3.82 | 4.57 | 4.55 | 4.37 | 4.01 | 3.93 | 3.67 | 3.74 | 4.38 | 3.77 | 4.49 |
| $K_2O$ | 4.50 | 4.73 | 4.72 | 4.97 | 4.38 | 4.57 | 4.60 | 4.69 | 4.67 | 4.75 | 4.64 | 4.62 | 4.74 | 4.69 |
| $H_2O$ total | 1.05 | 3.15 | 0.81 | 3.26 | 3.17 | 3.13 | 3.58 | 4.37 | 4.23 | 3.31 | 3.85 | 0.43 | 4.13 | 2.52 |
| F | 0.10 | 0.11 | 0.09 | 0.10 | 0.12 | 0.12 | 0.09 | 0.16 | 0.10 | 0.09 | 0.09 | 0.09 | 0.08 | 0.08 |
| Cl | 0.11 | 0.12 | 0.10 | 0.09 | 0.17 | 0.16 | 0.17 | 0.16 | 0.12 | 0.13 | 0.11 | 0.10 | 0.09 | 0.09 |
| Subtotal | 99.89 | 99.96 | 100.37 | 99.99 | – | 99.97 | – | – | – | 99.72 | 100.35 | 99.51 | 100.18 | 100.12 |
| $O=(F, Cl)_2$ | 0.07 | 0.07 | 0.06 | 0.06 | 0.09 | 0.09 | 0.08 | 0.10 | 0.07 | 0.07 | 0.06 | 0.06 | 0.05 | 0.05 |
| Total | 99.82 | 99.89 | 100.31 | 99.93 | – | 99.88 | – | – | – | 99.65 | 100.29 | 99.45 | 100.13 | 100.07 |
| Agpaitic index | 1.10 | 1.04 | 1.07 | 0.99 | 1.08 | 1.10 | 1.06 | 0.99 | 1.01 | 0.97 | 0.99 | 1.09 | 1.00 | 1.09 |

| | Older ring domes | | | | Younger ring domes | | | | 60,000-year southern arc lavas | | | | | | C. El Colli |
|---|---|---|---|---|---|---|---|---|---|---|---|---|---|---|---|
| Sample number | 89 | 92 | 133 | 37 | 108 | 79 | 174 | 175 | 105 | 83 | 115 | 73 | 40 | 67 | 15 |
| Eruptive unit | F | G | J | M | U | R | W | W | AA | BB | CC | DD | EE | EE | FF |
| Porphyritic (p) or aphyric (a) | p | p | p | p | a | p | p | a | a | a | a | a | a | a | a |
| $SiO_2$ | 75.22 | – | 74.51 | 75.34 | – | 75.11 | 75.08 | 76.14 | 76.16 | – | 76.81 | – | – | 76.82 | 76.67 |
| $TiO_2$ | 0.17 | 0.17 | 0.17 | 0.17 | 0.13 | 0.11 | 0.12 | 0.12 | 0.09 | 0.08 | 0.09 | 0.08 | 0.08 | 0.08 | 0.06 |
| $Al_2O_3$ | 11.61 | 11.42 | 11.49 | 11.53 | 11.46 | 11.17 | 11.09 | 11.43 | 11.64 | 11.73 | 11.66 | 11.65 | 11.67 | 11.65 | 11.82 |
| $Fe_2O_3$ | 0.92 | 0.86 | 0.76 | 0.87 | 0.79 | 0.92 | 0.88 | 0.84 | 0.65 | 0.74 | 0.69 | 0.71 | 0.66 | 0.65 | 0.56 |
| FeO | 1.16 | 1.16 | 1.28 | 1.25 | 0.98 | 0.86 | 0.88 | 0.95 | 0.83 | 0.74 | 0.80 | 0.76 | 0.81 | 0.81 | 0.67 |
| MnO | 0.07 | 0.06 | 0.07 | 0.07 | 0.05 | 0.05 | 0.05 | 0.05 | 0.04 | 0.04 | 0.04 | 0.04 | 0.04 | 0.04 | 0.04 |
| MgO | 0.05 | – | 0.05 | 0.04 | – | 0.04 | 0.04 | 0.05 | 0.03 | – | 0.03 | – | – | 0.03 | 0.02 |
| CaO | 0.25 | 0.27 | 0.28 | 0.28 | 0.22 | 0.18 | 0.19 | 0.24 | 0.24 | 0.23 | 0.23 | 0.23 | 0.23 | 0.23 | 0.30 |
| $Na_2O$ | 4.49 | 4.58 | 4.58 | 4.58 | 4.55 | 4.40 | 4.32 | 4.66 | 4.64 | 4.77 | 4.71 | 4.68 | 4.62 | 4.65 | 4.47 |
| $K_2O$ | 4.78 | 4.53 | 4.81 | 4.70 | 4.42 | 4.67 | 4.66 | 4.54 | 4.35 | 4.44 | 4.50 | 4.39 | 4.39 | 4.39 | 4.43 |
| $H_2O$ | 1.40 | 1.12 | 1.08 | 1.31 | 0.90 | 2.17 | 2.76 | 0.96 | 1.15 | 0.83 | 0.63 | 0.76 | 0.87 | 0.97 | 0.72 |
| F | 0.10 | – | 0.08 | 0.09 | 0.09 | – | 0.09 | 0.09 | 0.10 | 0.10 | 0.10 | 0.10 | 0.10 | 0.10 | 0.10 |
| Cl | 0.09 | – | 0.09 | 0.10 | 0.11 | – | 0.11 | 0.10 | 0.12 | 0.11 | 0.11 | 0.12 | 0.12 | 0.12 | 0.13 |
| Subtotal | 100.31 | – | 99.25 | 100.33 | – | – | 100.27 | 100.17 | 100.04 | – | 100.40 | – | – | 100.54 | 99.99 |
| $O=(F, Cl)_2$ | 0.06 | – | 0.05 | 0.06 | 0.06 | – | 0.06 | 0.06 | 0.07 | 0.07 | 0.07 | 0.07 | 0.07 | 0.07 | 0.07 |
| Total | 100.25 | – | 99.20 | 100.27 | – | – | 100.21 | 100.11 | 99.97 | – | 100.33 | – | – | 100.47 | 99.92 |
| Agpaitic index | 1.08 | 1.09 | 1.11 | 1.09 | 1.07 | 1.10 | 1.10 | 1.10 | 1.06 | 1.08 | 1.08 | 1.07 | 1.06 | 1.06 | 1.03 |

[a] $Na_2O$ and $K_2O$ were analyzed by J. Hampel, Univ. of Calif., Berkeley, using flame photometry. Total $H_2O$ was analyzed by S. Neil, U.S. Geological Survey, Menlo Park, using the Penfield method. F and Cl were analyzed by J. Thomas, University of Reading, Great Britain, using specific ion electrode techniques. The remainder of the elements were analyzed by the author using the methods of Carmichael et al. (1968). The samples were analyzed in duplicate and, in a few cases, in triplicate in order to assure that the small variations between eruptive groups were real. From these replicate analyses come the following estimates of precision: $SiO_2 \pm 0.1$ wt.%; $Al_2O_3$, $Na_2O$, $K_2O \pm 0.05$ wt.%; $Fe_2O_3$, $FeO \pm 0.02$ wt.%; $TiO_2$, MnO, MgO, $CaO \pm 0.01$ wt.%. $P_2O_5$ was less than 0.01 wt.% in all samples

[b] See Appendix 1 for sample descriptions (i.e., whether a sample is perlitic, pumiceous, or a dense glass)

[c] Eruptive unit letters are keyed to Fig. 1, except for gph, which refers to the giant pumice horizon and e, m, and l, which refers respectively to the early-, middle-, and late-erupted portions of the Tala Tuff

index = 0.98, Zr ≈ 500 ppm). In this regard, La Primavera is similar to Tertiary caldera complexes of the western United States (e.g., the Black Mountain and Silent Canyon centers (Christiansen and Noble 1965; Noble et al. 1968)) that produced ash flows zoned from peralkaline to subalkalic compositions, and to ring-dike complexes in New England (Billings 1956) and northern Nigeria (Jacobsen et al. 1958) where both peralkaline and metaluminous granites occur in the same center.

Ratios of the elemental abundances in the first-erupted portion of the Tala Tuff to those in the last-erupted portion are plotted in Fig. 3, following Hildreth (1979). This is equivalent to plotting the ratio of the abundance in the roof of the magma chamber to that in the deepest level tapped. Variations in trace-element abundances through the erupted volume of the Tala Tuff are more striking than for the major elements. Rb, Cs, Th, U, Sb, Nb, Ta, Sm, Gd, Tb, Tm, Yb, Lu, Y, Zr, Hf, and Zn are all enriched in the first-erupted portion of the Tala Tuff, whereas La, Ce, Nd, Ti, and Sc are enriched in the last-erupted part. As is true for the Bishop Tuff (Hildreth 1977, 1979), light rare earth elements (LREE) are depleted and heavy rare earth elements (HREE) are enriched roofward. Sr and Ba (among the most strongly-zoned elements in the Bishop Tuff) do not appear in Fig. 3 because in all samples they are below detection levels (10 and 20 ppm, respectively).

From the first-erupted through the last-erupted portion of the Tala Tuff, the molar ratio $Na_2O/(Na_2O+K_2O)$ drops from 0.60 to 0.54. The antithetic behavior of $Na_2O$ and $K_2O$ is common to a number of high-silica eruptive units, including the Bishop Tuff, the Bandelier Tuff (Smith 1979), and several ash flows from the Yellowstone Plateau (W. Hildreth, personal communi-

**Table 7.** Whole-rock neutron activation and X-ray fluorescence analyses[a]

| | Pre-caldera lavas | | | Tala Tuff | | | | | | | | Central domes and giant pumice horizon | | |
|---|---|---|---|---|---|---|---|---|---|---|---|---|---|---|
| Sample number | 290 | 193 | 90 | (186) | (323) | (184) | 255 | 256 | 210 | 252 | 218 | 317 | 234 | 283 |
| Eruptive unit | D | A | B | C | e | e | e | m | m | l | l | I | gph | H |
| Porphyritic (p) or aphyric (a) | a | p | a | p | a | a | a | a | a | p | p | p | p | p |
| INAA | | | | | | | | | | | | | | |
| La (1) | 55 | 46 | 76 | 50 | 38 | 40 | 37 | 52 | 47 | 66 | 64 | 66 | 80 | 79 |
| Ce (1) | 122 | 108 | 162 | 112 | 97 | 89 | 88 | 100 | 111 | 140 | 136 | 134 | 164 | 167 |
| Nd (6) | 50 | 45 | 64 | 47 | 46 | 54 | 44 | 58 | 43 | 54 | 54 | 54 | 60 | 65 |
| Sm (1) | 10.6 | 9.3 | 11.6 | 9.3 | 12.3 | 12.7 | 11.7 | 13.9 | 11.4 | 11.6 | 11.5 | 10.8 | 11.4 | 11.0 |
| Eu (7) | 0.09 | 0.07 | 0.10 | 0.07 | 0.08 | 0.12 | 0.06 | 0.11 | 0.05 | 0.07 | 0.06 | 0.06 | 0.11 | 0.12 |
| Gd (3) | 9.7 | 8.5 | 9.5 | – | – | – | 11.8 | 14.2 | 10.1 | 9.1 | 9.3 | 9.3 | 8.7 | 9.2 |
| Tb (2) | 1.57 | 1.49 | 1.54 | 1.46 | 2.51 | 2.50 | 2.36 | 2.68 | 1.83 | 1.60 | 1.57 | 1.62 | 1.49 | 1.55 |
| Tm (3) | 0.95 | 0.87 | 0.87 | – | – | – | 1.43 | 1.46 | 1.01 | 0.88 | 0.80 | 0.83 | 0.77 | 0.83 |
| Yb (1) | 5.9 | 6.2 | 6.0 | 6.0 | 10.3 | 10.5 | 10.0 | 10.9 | 7.3 | 6.0 | 6.0 | 5.9 | 5.6 | 5.5 |
| Lu (3) | 0.88 | 0.93 | 0.94 | 0.73 | 1.33 | 1.37 | 1.35 | 1.44 | 1.04 | 0.88 | 0.87 | 0.85 | 0.82 | 0.84 |
| Σ10 REE | 257 | 227 | 343 | – | – | – | 208 | 255 | 234 | 290 | 284 | 284 | 333 | 340 |
| Cs (3) | 3.2 | 3.6 | 3.0 | 3.5 | 6.2 | 6.2 | 6.6 | 6.2 | 7.1 | 3.5 | 4.1 | 3.6 | 3.5 | 3.3 |
| Th (2) | 18.3 | 17.8 | 16.8 | 17.8 | 27.1 | 26.4 | 25.8 | 27.6 | 20.5 | 19.0 | 18.2 | 18.9 | 17.3 | 17.7 |
| U (7) | 7.6 | 6.8 | 5.4 | 5.3 | 9.3 | 9.2 | 11.4 | 10.8 | 7.7 | 6.1 | 6.0 | 6.9 | 5.1 | 6.4 |
| Hf (1) | 14.5 | 13.2 | 14.6 | 13.5 | 20.6 | 19.4 | 19.8 | 19.7 | 14.8 | 13.2 | 12.7 | 13.2 | 14.5 | 14.9 |
| Ta (2) | 4.31 | 4.17 | 3.69 | 3.74 | 6.42 | 6.46 | 7.02 | 7.06 | 4.88 | 3.83 | 3.73 | 3.84 | 3.60 | 3.77 |
| Sc (1) | 0.63 | 0.93 | 1.79 | 1.01 | 0.45 | 0.40 | 0.42 | 0.71 | 0.80 | 1.01 | 0.92 | 0.98 | 0.83 | 0.81 |
| Fe %(1) | 1.36 | 1.19 | 1.56 | 1.28 | 1.36 | 1.35 | 1.32 | 1.41 | 1.26 | 1.28 | 1.33 | 1.36 | 1.42 | 1.37 |
| Co (10) | – | – | – | 0.7 | – | 0.3 | 0.4 | 0.7 | 0.6 | 0.4 | 0.7 | – | 0.4 | – |
| Sb (18) | 0.4 | 0.4 | < 0.9 | 0.4 | 0.7 | 0.7 | 0.7 | 0.9 | 0.4 | 0.5 | 0.4 | 0.4 | 0.4 | 0.5 |
| Mo (40) | – | – | – | 8 | 6 | 8 | – | – | – | – | – | – | – | – |
| W (30) | – | – | – | 2.0 | 5.4 | 4.9 | – | – | – | – | – | – | – | – |
| XRF | | | | | | | | | | | | | | |
| Rb (5) | 160 | 182 | 162 | 155 | 250 | 266 | 263 | 265 | 200 | 174 | 165 | 170 | 145 | 138 |
| Y (5) | 51 | 63 | 52 | 54 | 119 | 135 | 115 | 123 | 61 | 50 | 52 | 75 | 50 | 50 |
| Zr (5) | 500 | 439 | 616 | 455 | 592 | 596 | 575 | 590 | 457 | 519 | 482 | 521 | 645 | 667 |
| Nb (5) | 65 | 64 | 64 | 60 | 112 | 108 | 109 | 110 | 80 | 66 | 67 | 70 | 64 | 68 |
| Pb (5) | 21 | 26 | 18 | 20 | 25 | 27 | 37 | 42 | 22 | 18 | 19 | 24 | 16 | 18 |
| Zn (5) | 116 | 112 | 104 | 98 | 182 | 173 | 168 | 148 | 85 | 105 | 110 | 105 | 108 | 98 |

[a] Number in parentheses after element is standard deviation of analysis in percent. The samples in parentheses were analyzed at the Lawrence Berkeley Laboratory, California (LBL) by F. Asaro and H. Michel. R.L. Smith arranged for the rest of the samples to be analyzed by P. Baedecker at the USGS in Reston, Virginia. Duplicate analyses show systematic differences between LBL and USGS INAA analyses. To make all analyses directly comparable, the USGS analyses (those not in parentheses) have been multiplied by the following factors: Ce, 0.946; Sm, 1.099; Tb, 0.9025; Cs, 0.888; Hf, 0.919; Ta, 1.104; Sc, 0.884. R. Macdonald arranged for the XRF analyses to be performed at the University of Lancaster, England. The following elements were below the stated detection limits of XRF: Sr, 10; Ba, 50; and the LBL INAA: Au, 0.1; Ag, 1.2; Cd, 21; Ni, 18; Cr, 12; As, 9; Br, 6; Hg, 1 ppm

**Table 7** (continued)

| | Older ring domes | | | | Younger ring domes | | | | 60,000-year southern arc lavas | | | | | | C. El Colli |
|---|---|---|---|---|---|---|---|---|---|---|---|---|---|---|---|
| Sample number | 89 | 92 | 133 | (37) | 108 | 79 | (174) | 175 | 105 | 83 | (115) | 73 | 40 | 67 | 15 |
| Eruptive unit | F | G | J | M | U | R | W | W | AA | BB | CC | DD | EE | EE | FF |
| Porphyritic (p) or aphyric (a) | p | p | p | p | a | p | p | a | a | a | a | a | a | a | a |
| INAA | | | | | | | | | | | | | | | |
| La (1) | 79 | 81 | 80 | 82 | 56 | 51 | 56 | 60 | 38 | 39 | 40 | 40 | 39 | 38 | 35 |
| Ce (1) | 171 | 174 | 170 | 169 | 122 | 116 | 119 | 130 | 88 | 92 | 91 | 90 | 93 | 87 | 78 |
| Nd (6) | 62 | 65 | 64 | 68 | 48 | 49 | 54 | 51 | 35 | 37 | 40 | 39 | 39 | 38 | 35 |
| Sm (1) | 10.6 | 11.8 | 11.3 | 11.4 | 10.3 | 9.6 | 10.1 | 10.6 | 8.4 | 8.7 | 8.4 | 8.5 | 8.3 | 8.4 | 7.9 |
| Eu (7) | 0.12 | 0.11 | 0.12 | 0.13 | 0.09 | 0.08 | 0.09 | 0.09 | 0.06 | 0.06 | 0.07 | 0.06 | 0.05 | 0.06 | 0.03 |
| Gd (3) | 9.0 | 9.7 | 9.6 | – | 8.9 | 8.6 | – | 9.4 | 8.0 | 8.2 | – | 8.3 | 7.8 | 7.5 | 6.8 |
| Tb (2) | 1.46 | 1.46 | 1.47 | 1.46 | 1.53 | 1.50 | 1.53 | 1.53 | 1.35 | 1.37 | 1.37 | 1.34 | 1.33 | 1.35 | 1.24 |
| Tm (3) | 0.79 | 0.84 | 0.81 | – | 0.82 | 0.81 | – | 0.83 | – | 0.80 | – | 0.80 | 0.81 | 0.77 | 0.72 |
| Yb (1) | 5.7 | 5.8 | 5.8 | 6.0 | 5.9 | 5.8 | 6.3 | 6.0 | 5.5 | 5.8 | 5.8 | 5.7 | 5.6 | 5.5 | 5.4 |
| Lu (3) | 0.87 | 0.86 | 0.84 | 0.77 | 0.84 | 0.84 | 0.94 | 0.88 | 0.80 | 0.84 | 0.79 | 0.83 | 0.82 | 0.79 | 0.78 |
| Σ10 REE | 341 | 351 | 344 | – | 255 | 234 | – | 271 | – | 194 | – | 195 | 196 | 188 | 171 |
| Cs (3) | 2.8 | 2.8 | 2.9 | 2.8 | 3.4 | 3.4 | 3.2 | 3.2 | 3.4 | 3.5 | 3.6 | 3.7 | 3.6 | 3.5 | 4.4 |
| Th (2) | 17.3 | 17.5 | 17.2 | 17.5 | 17.5 | 17.4 | 18.2 | 17.9 | 16.6 | 17.1 | 17.2 | 16.6 | 16.5 | 15.9 | 19.4 |
| U (7) | 4.7 | 5.3 | 5.5 | 4.8 | 6.3 | 5.8 | 5.5 | 5.8 | 5.6 | 6.1 | 5.4 | 5.6 | 5.9 | 5.9 | 6.4 |
| Hf (1) | 15.1 | 15.3 | 14.9 | 15.1 | 14.0 | 14.5 | 14.2 | 14.5 | 11.2 | 11.3 | 11.2 | 11.4 | 11.4 | 11.2 | 8.8 |
| Ta (2) | 3.41 | 3.47 | 3.63 | 3.33 | 3.74 | 3.63 | 3.63 | 3.87 | – | 3.76 | 3.56 | 3.57 | 3.70 | 3.44 | 3.37 |
| Sc (1) | 1.04 | 1.06 | 1.05 | 1.04 | 0.67 | 0.67 | 0.69 | 0.74 | 0.70 | 0.70 | 0.71 | 0.69 | 0.68 | 0.69 | 1.09 |
| Fe %(1) | 1.62 | 1.62 | 1.61 | 1.61 | 1.37 | 1.35 | 1.39 | 1.41 | 1.13 | 1.15 | 1.14 | 1.14 | 1.13 | 1.13 | 0.93 |
| Co (10) | – | – | – | 0.32 | – | – | 0.16 | 0.2 | – | 0.3 | 0.5 | <0.5 | <0.2 | 0.5 | 0.2 |
| Sb (18) | 0.6 | <0.7 | 0.5 | 0.5 | 0.3 | 0.6 | 0.4 | 0.4 | 0.7 | 0.6 | 0.4 | <0.8 | <0.6 | 0.9 | 0.6 |
| Mo (40) | – | – | – | 10 | – | – | 4 | – | – | – | 6 | – | – | – | 4 |
| W (30) | – | – | – | 0.9 | – | – | 2.8 | – | – | – | 2.7 | – | – | – | 2.6 |
| XRF | | | | | | | | | | | | | | | |
| Rb (5) | 144 | 140 | 143 | 140 | 157 | 164 | 155 | 162 | 170 | 177 | 165 | 165 | 165 | 166 | 193 |
| Y (5) | 48 | 45 | 49 | 43 | 50 | 50 | 53 | 54 | 49 | 49 | 50 | 49 | 52 | 50 | 47 |
| Zr (5) | 682 | 657 | 675 | 660 | 548 | 584 | 560 | 568 | 373 | 381 | 375 | 382 | 367 | 377 | 226 |
| Nb (5) | 63 | 60 | 59 | 72 | 60 | 64 | 64 | 62 | 85 | 74 | 51 | 69 | 65 | 64 | 67 |
| Pb (5) | 17 | 19 | 16 | 21 | 25 | 26 | 18 | 28 | 25 | 18 | 16 | 31 | 25 | 24 | 15 |
| Zn (5) | 109 | 94 | 105 | 100 | 112 | 111 | 104 | 103 | 108 | 102 | 96 | 95 | 104 | 98 | 83 |

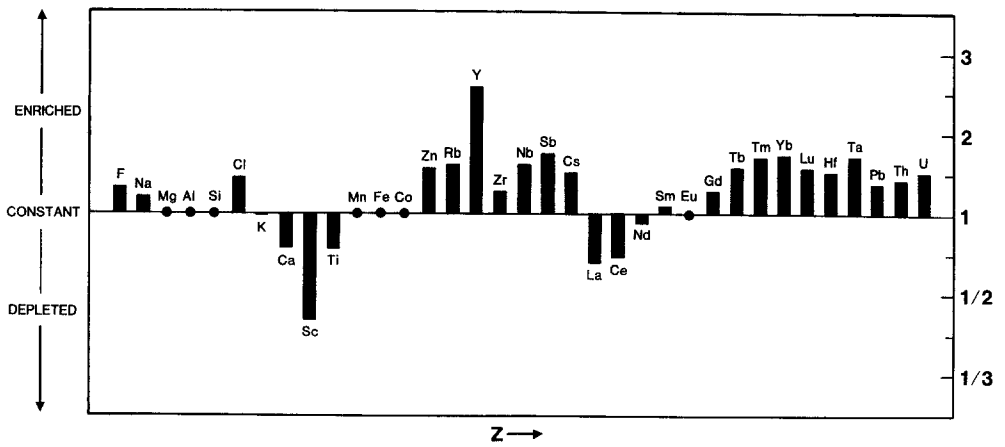


**Fig. 3.** Ash-flow enrichment and depletion factors. The elemental abundances in the first-erupted portion of the Tala Tuff are ratioed to those in the last-erupted part. If an element plots above the line it is enriched roofward, below the line it is depleted roofward, in each case by the factor on the right. Notice the cross-over in the behavior of the REE

cation, 1979). Wet-chemical analyses demonstrate that $TiO_2$ increases from 0.085 to 0.13 wt.%, whereas FeO*, MnO, and MgO are approximately constant at 1.70, 0.04, and 0.04 wt.%, respectively. Values for CaO are scattered, ranging from 0.14 to 0.25%, and show little correlation with stratigraphic position in the tuff. Alumina remains approximately constant through the erupted volume, but silica may be slightly depleted in the early-erupted portion of the tuff, presumably due to dilution by roofward concentrating Na, F, and Cl. Additional precise silica and water determinations are required to verify this observation. Despite possible losses on eruption, Cl, as well as F, is enriched in the first-erupted portion of the Tala Tuff, which contains

approximately 0.17 wt.% Cl and 0.12% F. Cl and F constitute about 0.11% and 0.09%, respectively, of the last-erupted portion of the Tala Tuff. This is consistent with analytical data from the Bishop Tuff (Hildreth 1979) and the Bandelier Tuff (R.L. Smith, personal communication, 1978), in which F and Cl were enriched in the cooler, more chemically evolved roof zones. Chlorine is enriched roofward in the strongly peralkaline Fantale Tuff as well (Gibson 1970).

### *Tala Tuff Magma Chamber*

Shortly after eruption of the Tala Tuff, two domes erupted through the center of the caldera lake, and the giant pumice horizon was deposited over the entire lake floor. Eruption of ring domes followed. All these events occurred within a time span unresolvable by K–Ar dating, about 5,000–10,000 years (Mahood 1980a, b).

The last-erupted portion of the Tala Tuff is compositionally nearly identical to the south-central dome (compare Samples 252 and 218 with Sample 317 in Tables 6 and 7), whereas the north-central dome and older ring domes are slightly more mafic in composition. This indicates continuity in compositional gradients from that part of the magma chamber that erupted explosively as the Tala Tuff to that which erupted as early post-caldera lavas. Similar relations (i.e., the earliest post-caldera lavas being similar to or lying on slightly more mafic extension of the chemical trends in the ash flows) have been documented in several large silicic systems: Long Valley, California (Bailey et al. 1976), the Valles caldera, New Mexico (Smith 1979), and Yellowstone (Hildreth et al. 1980). In all these examples, ring domes presumably represent the tapping of slightly deeper portions of the compositionally zoned magma chamber from which the ash flow erupted.

Trends for most elements are unidirectional from the first-erupted portions of the Tala Tuff to the older ring domes (Fig. 4); HREE, Ta, Rb, Cs, Th, U, Zn, Nb, Y, Sb, and W are enriched roofward, whereas LREE, Ti, Mn, and Sc are enriched in the deeper levels of the magma chamber. Certain elements, however, show a reversal in trend. Zr and Hf are depleted in the last-erupted portion of the Tala Tuff and the south-central dome, but increase again in the north-central and older ring domes. Similarly, $Na_2O$ is depleted in the last-erupted portion of the Tala Tuff relative to both the first-erupted portion of the tuff and the immediately-post-collapse lavas. Iron appears unzoned in the ash flow, but, like Zr, Hf, and Na, it is more abundant in the north-central dome and older ring domes. The reversals in Na, Zr, and Hf parallel the trend in the agpaitic index, which is 1.10 in the first-erupted portion of the Tala Tuff, falls to approximately 0.99 in the last-erupted portion, and then rises to approximately 1.10 in the older ring domes.

There is a similar lack of continuity in the compositions of phenocrysts in the earliest post-caldera lavas. The ferrohedenbergite and fayalite of the north-central dome are more magnesian and the sanidine is more sodic than in the south-central dome (Fig. 2). These phenocryst trends, however, do not extend to the older ring domes, which presumably represent the eruption of slightly deeper, hotter, less-evolved magma from a zoned magma chamber; ferrohedenbergite and sanidine phenocrysts in the older ring domes are intermediate in composition between those of the south- and north-central domes.

These reversals may have been present within a continuously-zoned magma chamber, reflecting contrasting differentiation mechanisms and conditions in the volatile-enriched roof zone that erupted as the Tala Tuff and in the relatively drier, slightly hotter, deeper magma that erupted later as the older ring domes. Alternatively, immediately following caldera collapse, the new roof-zone magma may have been temporarily out of equilibrium with its surroundings. The rapid evacuation of the Tala Tuff magma and, shortly thereafter, the magma of the central domes and the giant pumice horizon, would lead to a rapid reorganization of the magma chamber, with magma from deeper levels becoming the most roofward. A free vapor phase may have been present as a result of vesiculation during the caldera-producing eruption. During this period of re-establishment of magma-chamber equilibrium, transient mechanisms may have produced the increase in Na, Fe, Zr, and Hf in the magma that erupted as the north-central dome and older ring domes. Perhaps the less-magnesian ferrohedenbergite and less-sodic sanidine of the older ring domes did not precipitate until after the eruption of the Tala Tuff and so reflect conditions in the newly-formed roof zone of the magma chamber.

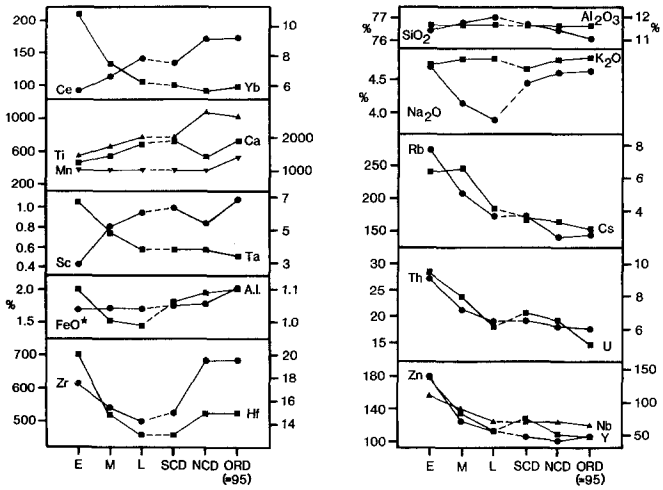


**Fig. 4.** Elemental trends in the Tala Tuff and immediately post-collapse lavas. *E, M,* and *L* stand for the early-, middle-, and late-erupted portions of the Tala Tuff, respectively, while *SCD, NCD,* and *ORD* refer to the south-central, north-central, and older (95,000-year) ring domes, respectively. *A.I.* agpaitic index

## Post-95,000-Year Evolution of the Primavera Magma Chamber

Since the eruption of the 95,000-year ring domes, the lavas have become progressively more silicic and less peralkaline (Fig. 5). Values for FeO*, $TiO_2$, MgO, and MnO in the older ring domes are approximately twice those in the most recently-erupted unit, Cerro El Colli (Sample 15 in Tables 6 and 7). Although there is some scatter in the alkali data due to mobility on post-eruptive hydration, $Na_2O$ remained approximately constant while $K_2O$ decreased from about 4.8 to 4.5% (water-free) with time. Cl concentrations appear to have increased slightly from 0.09 wt.% in the perlitic and pumiceous older ring domes to 0.13% in the youngest of the southern arc obsidians, but this may reflect better retention of Cl by obsidian samples. F remained approximately constant at about 0.10%. The data for $Al_2O_3$ and CaO are less systematic than for the other elements. The variation is much greater than that attributable to analytical uncertainty, and the positive correlation between the two elements suggests that it is real.

Rb, Cs, and possibly U are the only trace elements that increased monotonically with time in the lavas (Fig. 5); nearly

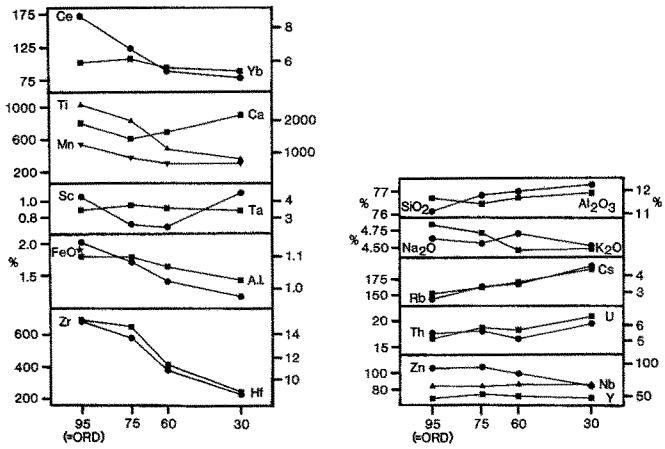


**Fig. 5.** Elemental trends in the post-Tala lavas. This figure is similar to Fig. 4. *95:* older ring domes (ORD of Fig. 3); *75:* younger ring domes; *60:* 60,000-year southern arc lavas; *30:* the youngest southern arc lava, Cerro El Colli, erupted approximately 30,000 years ago. With increasing differentiation, only Si, Rb, Cs, and possibly U are systematically enriched, while all other elements decrease or remain approximately constant

all other trace elements decreased (REE, Zr, Hf, Mn, Co, and Zn) or remained approximately constant (Sb, Ta, Nb, Pb, and Y). Sc values, like Ca, are scattered, and Th, which remained approximately constant in the 95,000-, 75,000- and 60,000-year lavas, increased in Cerro El Colli, the youngest dome.

In Fig. 6, the elemental abundances in Cerro El Colli are ratioed to those in the older ring domes. This diagram is not strictly comparable to the enrichment-factor diagram for the Tala Tuff (Fig. 3) because it does not represent the chemical zonation present in the magma chamber at one moment in time; rather, it is thought to illustrate the chemical evolution through time of the most roofward magma in the chamber. The difference between the two enrichment patterns is striking; with increasing differentiation, the ash-flow magma was enriched in the HREE and many of the multivalent cations, whereas the post-caldera lavas were enriched systematically only in Si, Rb, Cs, and possibly U. (Th plots above the no-enrichment line only because of its increase in Cerro El Colli.) The increase in silica content at the expense of the femic components and the decrease in peralkalinity in the post-caldera lavas represent a trend toward the "minimum melt" composition in the granitic system. In terms of melt structure, this implies the development of an increasingly-polymerized Si–Al network which contains only enough alkalies for local charge balance of aluminum.

Both the phenocryst compositions and the bulk chemistry of the younger ring domes are similar to the pre-caldera lavas. This suggests that, following the eruption of the Tala Tuff, it took approximately 20,000 years to re-establish conditions in the magma similar to those during eruption of the pre-caldera lavas. In the approximately 5,000 years between eruption of the pre-caldera Mesa El León dome and the Tala Tuff, the system rapidly acquired a volatile-rich cap enriched in multivalent cations. Such concentration did not occur following eruption of the younger ring domes; on the contrary, in subsequent lavas most trace metals decreased in concentration.

## Evaluation of Differentiation Mechanisms

The homogeneity of phenocryst and whole-rock compositions within each post-caldera eruptive group, along with the arcuate arrangement of vents, is strong evidence that these lavas erupted from a single unified magma chamber. Trends in the post-caldera lavas, however, do not reflect the tapping of a static zoned magma chamber. Studies of large-volume zoned ash-flow eruptions (Lipman et al. 1966; Byers et al. 1976; Smith and Bailey 1966; Hildreth 1977, 1979; Smith 1979) have shown that magma at the roof of a chamber is generally more differentiated and poorer in phenocrysts than at deeper levels. The Primavera trend is opposite to that expected on tapping successively deeper levels; the last lavas erupted are phenocryst-free and are the most siliceous. The preferred interpretation is that the Tala Tuff and all the post-caldera lavas erupted from a magmatic system that was evolving chemically with time. If the geometry of the magma chamber changed (e.g., the southern arc lavas may represent a southward expansion of the magma chamber), the magma chamber was (is) presumably large enough that magma in its roof zone did not immediately "feel" the effects of new additions below. Thus changes in composition within a sequence of lavas reflect high-level differentiation mechanisms.

In the following discussion, differentiation mechanisms commonly proposed to explain chemical trends in silicic magmas will be discussed as they apply to La Primavera. Because there is no positive evidence of a unitary magma chamber during eruption of the pre-caldera lavas, they will not be considered further.

### *Crystal Fractionation*

*Physical Constraints on Crystal Settling.* Most of the Tala Tuff and many of the Primavera lavas are aphyric. If crystal settling

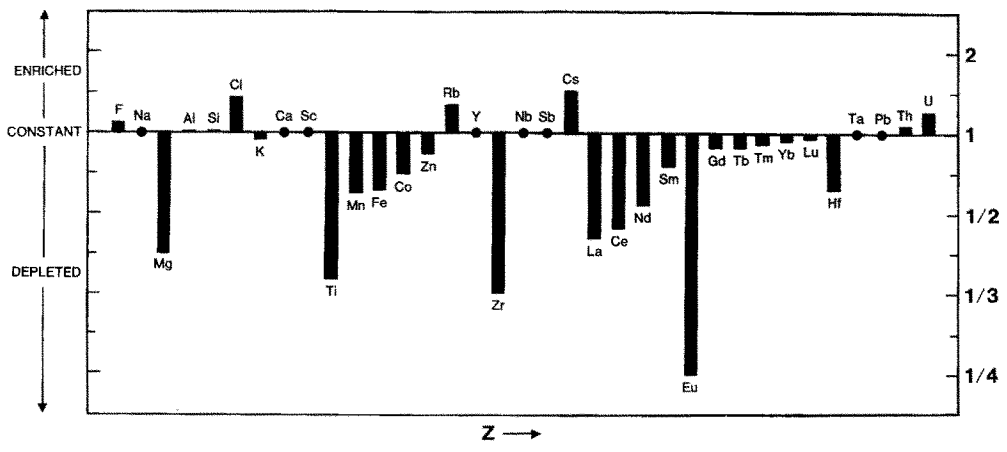


**Fig. 6.** Enrichment and depletion factors in the post-caldera lavas. The elemental value in the youngest southern arc lava, Cerro El Colli, is ratioed to the average of the older ring domes. This figure is not strictly analogous to Fig. 3 as it does not represent the zonation present in the magma chamber at any one point in time; rather it presumably illustrates the evolution through time of the most roofward magma

operated in these magmas, either all the phenocrysts settled out or the magmas became superheated prior to eruption and the phenocrysts were resorbed. Phenocrysts show no evidence of having settled; they are euhedral, unzoned, and homogeneous.

Assuming that magma for any single eruptive group is drawn over an area of 150 $km^2$, phenocrysts must settle through at least 33 m to produce 5 $km^3$ of aphyric magma. This is a minimum value because lavas probably do not draw down the magma chamber uniformly, but rather tap to somewhat deeper levels over a more localized area. Settling velocities of the smaller mafic phenocrysts are too slow to sink that distance in the 15,000–30,000 years between eruptive episodes if the melt contains less than approximately 1.5 wt.% water. Diffusion often has been discarded as a viable differentiation mechanism in silicic melts because of its reputed slowness, yet diffusion distances in relatively dry rhyolitic melts are similar to and, in some cases, greater than the distance small mafic phenocrysts can settle in the same period of time.

*Chemical Constraints.* Repeated tapping of a cooling homogeneous magma chamber that is crystallizing inward from its margins is equivalent geochemically to settling of the observed phenocryst phases; thus the chemical constraints on both of these differentiation mechanisms are similar.

The compositional zonation present in the magma chamber just prior to eruption of the Tala Tuff was not the product of crystal fractionation alone for the following reasons: (1) Trace elements were substantially zoned in the near absence of major-element zonation. The nearly two-fold roofward enrichment of elements such as Nb, Y, Ta, U, Rb, and Cs would require removal of at least half the magma as phenocrysts. But this would have profound effects on major elements such as Ca and Fe, effects that are not observed. (2) Zn was enriched and Sc and Ti were depleted roofward, while Fe, Mg, and Mn were unzoned. This separation of transition metals is incompatible with the removal of mafic phenocrysts, which are strongly enriched relative to glass in these elements.

Separation of phenocrysts in their modal proportions would not produce the chemical trends in the post-caldera lavas. Removal of sanidine would lead to increasingly peralkaline residual melts, the opposite of the trend observed. The weighted average MnO/FeO* ratio is larger for the mafic minerals than for the bulk lavas, so separation of mafic phenocrysts would lead to a decrease in whole-rock MnO/FeO* with time. Yet the MnO/FeO* ratio remains constant in the post-caldera lavas. Approximately 15–20% of the Ca and 20–25% of the Sc of porphyritic rocks resides in ferrohedenbergite; removal of ferrohedenbergite in its modal proportion in quantities sufficient to deplete the younger lavas in FeO* would deplete the whole-rock in Ca and Sc, trends not observed.

Crystal fractionation models for the post-caldera lavas were calculated using the computer program of Wright and Doherty (1970) and electron-microprobe analyses of the phenocrysts present in the assumed parent magmas. Solutions require 1–30% fractionation. Sums of the least-squares residuals are quite small, but this is a necessary consequence of only slight changes in composition from parent to daughter magmas. Although moderately successful fits for individual elements were obtained, the solutions suffer from the following shortcomings:

(1) More than half the test cases yield solutions requiring both the addition and subtraction of phases, a result that seems geologically improbable, especially in crystal-poor rhyolites.

(2) By manipulating three mafic phases (fayalite, ferrohedenbergite, and ilmenite) the resulting residuals for Fe, Ti, and Mn are small, but in order not to deplete the daughter magmas in Ca, the amount of ferrohedenbergite removed must be minimized, and fayalite and ilmenite must be removed in proportions far greater than their mode. This is inconsistent with relative crystal sizes, which dictate that ferrohedenbergite should settle ten times faster than the smaller fayalite and ilmenite.

(3) The observed decrease in $K_2O$ from older to younger magma is invariably greater than that calculated by the best fit and reflects the impossibility of decreasing bulk $K_2O$ while maintaining $Na_2O$ and $Al_2O_3$ approximately constant by separation of sodic sanidine.

The best computer solutions based on major elements were then tested to see if they predicted correct trace-element concentrations in the daughter magmas. Sanidine, ferrohedenbergite, fayalite, and ilmenite partition coefficients determined in this study and zircon partition coefficients from the Bishop Tuff (Hildreth 1977, p. 118, Sample 77) were used in the calculations. An amount of zircon necessary to produce the observed changes in Zr was assumed, but the required amounts of zircon (2 to $4 \times 10^{-4}$ of the magma) are probably geologically unreasonable.[1] Because of the uncertainty in the zircon concentration, the trace-element calculations were made both with and without zircon as a separating phase. Examples of these calculations appear in Table 8.

Agreement between predicted and measured concentrations of most trace elements in the daughter magmas is poor. Most trace elements decrease or remain approximately constant with time in the post-caldera lavas, but the calculations yield increasing concentrations. This is a result of the large proportion of sanidine and quartz in the separating phases which, despite the strong enrichment of elements such as the LREE and Zn in the mafic phases, causes the bulk distribution coefficients (D) for most elements to be less than one. Participation of zircon improves the fit slightly, predicting HREE abundances similar to those observed and decreasing the amount of enrichment predicted for some elements. At higher amounts of crystal fractionation (e.g., second example in Table 8), the hypothetical fixed amount of zircon is a smaller proportion of the separating phases and, therefore, the bulk distribution coefficients for many elements decrease, including $D_{Yb}$ which falls to less than one. In all the calculated models, the removal of phenocryst phases does not produce the observed decrease in LREE with time. Also, despite the dominant role of sanidine in the calculated models and $D_{Eu}$ for all cases being greater than one, the predicted decrease in Eu is always smaller than that observed.

### *Partial Melting*

Progressive melting of a source region would not produce the trends observed in the post-caldera lavas. Initial partial melts would be enriched in Si, Rb, and Cs and depleted in Fe, Mg, and Ti relative to subsequent melt-fractions. The reverse is observed in the post-caldera lavas; they become increasingly siliceous and depleted in the mafic elements with time.

Hildreth (1977, p. 233–249) demonstrated that many aspects of the chemical zonation in the Bishop Tuff cannot have resulted from accretion of successive partial melt increments. Many of his arguments apply equally well to the Tala Tuff, the two most

1 Most eruptive units contain no zircon and, in those that do, zircon is present at the level of several ppm. Assuming that Hf in the whole-rock in excess of that in the separated glass resides in zircon, approximately $3 \times 10^{-5}$ of the magma can be zircon for Samples 37 and 79. This value is a maximum because the mafic phenocrysts contain significant amounts of Hf

**Table 8.** Trace-element test of crystal fractionation[a]

Parent magma: Sample 37—95,000-year ring dome
Daughter magma: Sample 79—75,000-year ring dome

| | | |
|---|---|---|
| Wt.% of parent magma subtracted: | | 8.96 |
| Wt.% of the phases subtracted: | Qtz: | 15.18 |
| | San: | 73.44 |
| | Cpx: | 6.70 |
| | Fa: | 3.12 |
| | Ilm: | 1.34 |
| | Zr: | 0.22 |

| | Ce | Sm | Eu | Yb | Rb | Th | U | Hf | Ta | Sc | Zn |
|---|---|---|---|---|---|---|---|---|---|---|---|
| [D] with zircon | 0.421 | 0.518 | 1.88 | 1.43 | 0.264 | 0.223 | 0.696 | 5.88 | 0.443 | 7.87 | 0.959 |
| [D] without zircon | 0.370 | 0.479 | 1.86 | 0.349 | 0.264 | 0.086 | 0.040 | 0.054 | 0.322 | 7.74 | 0.959 |
| [C] parent | 169 | 11.4 | 0.13 | 6.0 | 140 | 17.5 | 4.8 | 15.1 | 3.33 | 1.04 | 100 |
| [C] daughter predicted with zircon | 178 | 11.9 | 0.12 | 5.8 | 150 | 18.8 | 4.9 | 10.5 | 3.50 | 0.64 | 100 |
| [C] daughter predicted without zircon | 179 | 12.0 | 0.12 | 6.4 | 150 | 19.1 | 5.3 | 16.5 | 3.55 | 0.65 | 100 |
| [C] daughter measured | 116 | 9.6 | 0.08 | 5.8 | 164 | 17.4 | 5.8 | 14.5 | 3.63 | 0.67 | 111 |

Parent magma: Sample 79—75,000-year ring dome
Daughter magma: Sample 67—60,000-year southern arc lava

| | | |
|---|---|---|
| Wt.% of parent magma subtracted: | | 33.43 |
| Wt.% of the phases subtracted: | Qtz: | 34.94 |
| | San: | 60.75 |
| | Cpx: | 0.84 |
| | Fa: | 2.75 |
| | Ilm: | 0.60 |
| | Zr: | 0.12 |

| | Ce | Sm | Eu | Yb | Rb | Th | U | Hf | Ta | Sc | Zn |
|---|---|---|---|---|---|---|---|---|---|---|---|
| [D] with zircon | 0.835 | 0.393 | 1.60 | 0.703 | 0.207 | 0.204 | 0.393 | 3.26 | 0.203 | 1.92 | 0.509 |
| [D] without zircon | 0.807 | 0.372 | 1.59 | 0.115 | 0.207 | 0.129 | 0.035 | 0.079 | 0.137 | 1.85 | 0.509 |
| [C] parent | 116 | 9.6 | 0.08 | 5.8 | 164 | 17.4 | 5.8 | 14.5 | 3.63 | 0.67 | 111 |
| [C] daughter predicted with zircon | 123 | 12.0 | 0.07 | 6.4 | 223 | 23.7 | 7.3 | 8.26 | 4.95 | 0.51 | 133 |
| [C] daughter predicted without zircon | 124 | 12.2 | 0.07 | 8.2 | 223 | 24.5 | 8.6 | 21.0 | 5.10 | 0.52 | 133 |
| [C] daughter measured | 87 | 8.4 | 0.06 | 5.5 | 166 | 15.9 | 5.9 | 11.2 | 3.44 | 0.69 | 98 |

[a] D is the bulk distribution coefficient for the separating phases. C is the concentration of an element in ppm

critical lines of reasoning being that the strong partitioning of both LREE and HREE into accessories, such as apatite or zircon, and of the first transition series metals into the ferromagnesian phases requires that the elements of each group observe a common trend (but not magnitude) of enrichment or depletion in successive melt increments. Thus incremental partial melting does not readily explain the crossover in REE on the enrichment factor diagram (Fig. 3) nor the divergent enrichment directions of the first transition series elements.

### Phenocryst/Glass Partitioning and Melt Structure

Because crystal fractionation during partial melting or due to crystal settling cannot be the dominant mechanism responsible for the compositional gradient in the Tala Tuff or the trends with time in the post-caldera lavas, other processes must be involved. The progressive increase in the proportion of network-forming elements to network-modifying elements in the post-caldera lavas suggests that trace-element behavior may be related to changing melt structure. The term "melt structure" as used here refers to the mutual spatial relationship between atoms in a silicate liquid. Because melts lack long-range order, a melt structural state is characterized by an *average* concentration of variously coordinated cations (e.g., a highly polymerized melt has, on the average, fewer octahedral "sites" than a less polymerized melt). In this statistical sense, the melt structure is defined at any given combination of pressure, temperature, volatile content, and bulk composition.

Melt structure is thought to be a function of temperature, pressure, oxygen fugacity, and bulk composition, which includes the important effect of the concentration of volatiles dissolved in the magma (Burnham 1975; Virgo et al. 1980; Mysen et al. 1980). Crystal/liquid partition coefficients depend on the composition of the phenocryst phase as well as melt structure (Häkli and Wright 1967; Schnetzler and Philpotts 1970; Watson 1977; Takahashi 1978; Hart and Davis 1978; Ryerson and Hess 1978; Watson 1979; Mysen and Virgo 1980). As discussed previously, the temperature, oxygen fugacity, and pressure of the Primavera magmas are thought to have varied little between eruptive groups. Compositions of the mafic phenocrysts in the different groups are nearly identical, and the range of sanidine compositions is small. Thus changes in melt structure and partition coefficients between eruptive units are largely a function of changing bulk composition. One might "measure" the effect of these small changes in bulk composition on melt structure by determining variations in phenocryst/glass partition coefficients between

**Table 9.** Summary of phenocryst/glass partition coefficients[a]

| | Sanidine | | | | Ferrohedenbergite | | | | Fayalite | | | Ilmenite |
|---|---|---|---|---|---|---|---|---|---|---|---|---|
| Sample No. | 193 | 218 | 37 | 79 | 193 | 317 | 37 | 79 | 317 | 37 | 79 | 37 |
| Eruptive unit[b] | PCD | TT | ORD | YRD | PCD | SCD | ORD | YRD | SCD | ORD | YRD | ORD |
| La | 0.06 | 0.037 | 0.057 | 0.11 | 23 | 2.9 | 3.5 | 24 | 1.08 | 2.0 | 23 | 1.31 |
| Ce | 0.033 | 0.031 | 0.043 | 0.095 | 20.9 | 3.5 | 4.0 | 21.6 | 0.93 | 1.78 | 20.4 | 1.19 |
| Nd | 0.01 | 0.02 | 0.04 | 0.09 | 16 | 5.3 | 5.9 | 17 | 0.77 | 1.5 | 14 | 0.96 |
| Sm | 0.019 | 0.020 | 0.029 | 0.946 | 14 | 6.2 | 6.2 | 13 | 0.496 | 1.060 | 8.4 | 0.684 |
| Eu | 2.3 | 2.3 | 2.0 | 2.2 | 12 | 5 | 6 | 10 | 0.1 | 0.4 | 5.8 | 0.4 |
| Tb | 0.012 | 0.016 | 0.023 | 0.022 | 6.9 | 5.0 | 4.0 | 6.1 | 0.31 | 0.54 | 2.8 | 0.36 |
| Dy | 0.01 | 0.02 | 0.02 | 0.02 | 6 | 4.5 | – | 4.8 | 1 | 1 | 3 | 0.4 |
| Yb | 0.005 | 0.014 | 0.016 | 0.018 | 6.4 | 5.0 | 4.5 | 5.5 | 0.92 | 0.98 | 1.96 | 0.55 |
| Lu | 0.008 | 0.010 | 0.015 | 0.014 | 8 | 6.9 | 6.1 | 7 | 1.3 | 1.3 | 2.2 | 0.72 |
| Th | 0.010 | 0.017 | 0.021 | 0.025 | 3.44 | 0.36 | 0.77 | 2.89 | 0.276 | 0.438 | 3.17 | 0.43 |
| U | 0.008 | 0.021 | 0.018 | 0.014 | 1.0 | 0.12 | 0.33 | 0.87 | 0.12 | 0.13 | 0.69 | 0.06 |
| Hf | 0.005 | 0.018 | 0.015 | 0.015 | 1.52 | 0.30 | 0.39 | 2.04 | 0.12 | 0.28 | 1.78 | 0.65 |
| Ta | 0.004 | 0.018 | 0.018 | 0.015 | 0.69 | 0.10 | 0.97 | 0.49 | 0.098 | 0.090 | 0.575 | 18.0 |
| Sc | 0.04 | 0.04 | 0.05 | 0.06 | 133 | 110 | 109 | 172 | 5.1 | 4.8 | 9.3 | 18 |
| Ti | 0.1 | 0.05 | 0.11 | 0.11 | 2.6 | 4 | 2.5 | 2.5 | 0.3 | 0.4 | 0.5 | 380 |
| Mn | 0.011 | 0.020 | 0.018 | 0.020 | 34 | 30 | – | 33 | 63 | 56 | 77 | 27 |
| Fe | 0.14 | 0.14 | 0.11 | 0.14 | 20 | 18 | 15 | 18 | 37 | 33 | 40 | 24 |
| Co | 0.3 | 0.4 | 0.3 | 0.2 | 9 | 9 | 17 | 6 | 9 | 23 | 6 | 26 |
| Zn | 0.04 | 0.06 | 0.06 | 0.07 | 21 | 8.9 | 7.2 | 14.8 | 11.1 | 10.4 | 10.7 | 7.8 |
| Mo | 0.2 | 0.0 | 0.2 | 0.5 | – | – | – | – | 0.1 | 1.4 | 1.2 | 11 |
| Rb | 0.39 | 0.31 | 0.36 | 0.34 | – | – | – | – | – | – | – | – |
| Cs | 0.012 | 0.023 | 0.009 | 0.028 | – | – | – | – | – | – | – | – |

[a] The calculated errors on the partition coefficients, the method of correcting for impurities in the mineral separates, and the INAA analyses of the separated glass and phenocrysts are given in Mahood (1980a)

[b] PCD = pre-caldera dome, TT = Tala Tuff, SCD = south-central dome, ORD = older (95,000-year) ring dome, YRD = younger (75,000-year) ring dome

the older and younger ring domes and between the ring domes and the Tala Tuff and its outgassed equivalent, the south-central dome.

With this reasoning in mind, seventeen mineral and glass separates from five representative La Primavera samples were analyzed at Lawrence Berkeley Laboratory by INAA. The resulting analyses and partitioning patterns are discussed elsewhere (Mahood 1980a; Mahood and Hildreth, in preparation); the pertinent partition coefficients are summarized in Table 9. Despite only minor differences in the major-element compositions of phenocrysts, the concentrations of many of the trace elements vary by factors of 5 to 10 among analyzed samples. This is reflected in crystal/glass partition coefficients that differ by as much as a factor of 20. These differences are surprisingly large; the variation in the ferrohedenbergite partition coefficients for LREE in the Primavera magmas is about as great as the entire range of clinopyroxene partition coefficients reported from basaltic to rhyodacitic magmas (Arth 1976).

*Phenocryst/Glass Partitioning in the Older and Younger Ring Domes and the Chemical Evolution of the Post-Caldera Lavas*

All the southern arc lavas are aphyric, so discussion of the chemical evolution of the post-caldera lavas as reflected in trace-element partitioning is necessarily restricted to the older and younger ring domes. The behavior of trace-element partition coefficients in the ring domes is systematic. Fayalite partition coefficients for REE, Th, U, Hf, Ta, Sc, and Mn are greater in the younger ring dome (Sample 79) than in the older ring dome (Sample 37), while, within the limits of error, partition coefficients for Ti, Co, Zn, and Mo are the same in both samples. Sanidine partition coefficients for La, Ce, Nd, Sm, and Th are greater in the younger ring dome, whereas values for Eu, Tb, Dy, Yb, Lu, Rb, Cs, U, Hf, Sc, Ti, Mn, Fe, Co, Zn, and Mo are similar in the two samples within the rather large range of error. Ferrohedenbergite partition coefficients for La, Ce, Nd, Sm, Eu, Tb, Yb, Th, U, Hf, Sc, and Zn are greater in the younger ring dome, whereas, within the limits of error, Lu and Ti are the same in both. The only clinopyroxene partition coefficient that is smaller in the younger ring dome is that for Ta. This single exception to constant or increasing partition coefficients with time, however, might be an artifact of the correction of Ta abundance in ferrohedenbergites for ilmenite inclusions.

The observed decrease in the concentration of network modifiers Fe, Mn, Mg, and K (in the case of these peralkaline melts) in the sequence of post-caldera lavas would be expected to foster increasing polymerization of the melts and, as a result, increasing crystal-liquid partition coefficients. The increases in partition coefficients for many elements from the older to the younger ring dome, however, seem remarkably large considering the small changes in major-element composition. From such behavior one can make the following inferences:

(1) High-silica rhyolitic melts are so strongly polymerized that small changes in major-element composition greatly affect the number of "sites" in the liquid suitable for most trace elements. Small distortions of the silicate network may make already marginal sites even less energetically favored.

(2) The increase in partition coefficients may reflect increasing melt polymerization and resultant decrease in melt trace-metal sites due chiefly to a decrease in the concentration of volatiles dissolved in the melt. There is no direct way of estimat-

ing the original volatile contents of the 95,000- and 75,000-year magmas because they lack hydrous phases, but the similarity in phenocryst abundance, assemblage, and composition suggests that the absolute difference in volatile content between the magmas of the two eruptive groups could not have been large. Certainly there is no indication in the chemical analyses (Table 6) of a significant difference in F and Cl concentration between the two groups of magmas. However, at low water or fluorine concentrations, small variations have large effects, as illustrated by the rapid drop in liquidus temperature on addition of small amounts of water or fluorine to the anhydrous granitic system (Wyllie and Tuttle 1961; Naney and Swanson 1980).

(3) If trace elements are complexed by hydroxyl, fluoride, chloride, phosphate, sulfate, or carbonate ligands in silicate melts, any decrease in concentration of these complexing agents would increase the activity of the trace elements in the melt, thereby favoring increased concentrations in the crystalline phases. Complexing might lead to discontinuities in crystal/liquid partitioning behavior; partition coefficients might remain low as long as the concentration of the complexing ligands is sufficient to complex most of the trace metals, but once the concentration of complexing ligands falls below that threshold, the partition coefficients will rise. This mechanism might be most effective in relatively volatile-poor high-silica magmas where the total concentration of possible complexing ligands is of the same order as the sum of the network modifiers (which includes most trace elements).

Complexes involving other cations may also be important in increasing the solubility of trace metals in melts. For example, Watson (1979) has suggested, on the basis of measurements demonstrating an increase in the solubility of Zr with increasing agpaicity of the melt, that Zr is associated with the alkalies as complexes.

The mechanism(s) responsible for the observed changes in partition coefficients from the older to younger ring domes cannot yet be identified unambiguously. In fact, the very existence of trace-metal complexes within silicate melts has not been experimentally verified. The suggested mechanisms are not mutually exclusive, however, and it is possible that all three operated in the post-caldera lavas.

*Migration of Elements to Structurally More Favorable Melts.* All such mechanisms rely on some change in melt structure that, by increasing the chemical potential of trace metals in the melt, produces larger partition coefficients. Increased partitioning of trace metals into phenocrysts, however, alters only the location of elements within the magma, not the whole-rock abundances, and, therefore, would not explain the decrease in whole-rock (and glass) abundances of most trace metals with time in the post-caldera lavas. The combined effects of gradients in temperature, bulk composition, and volatile content should logically result in a magma chamber with a gradient in melt structure. In the relatively dry post-caldera system, the combined gradients could have been such that the roof was more polymerized than the more-mafic, hotter, deeper levels. The progressive decrease with time of whole-rock (and glass) trace-element abundances in the post-caldera lavas (each of which presumably represented the uppermost and most-differentiated magma in the Primavera magma chamber at the moment of its eruption) may have been accomplished by migration of these elements out of the roofward magma into deeper, less polymerized levels of the magma chamber.

The two-liquid partitioning studies of Watson (1976) and Ryerson and Hess (1978) on immiscible mafic and silicic melts are examples of diffusion into a structurally more favorable melt. They found that Ti, Fe, Mn, Mg, Ca, P, Zr, Ta, Cr, REE, Sr, and Ba are partitioned into the less-polymerized mafic melt and that Al, Na, K, and Cs are preferentially concentrated in the silicic melt. The progressive enrichment of the post-caldera magmas in only Si, Rb, and Cs, while all other elements remain approximately constant or decrease in concentration, is analogous to the partitioning of all cations but aluminum and the alkalies into the less-polymerized mafic melts in the two-liquid experiments. Aluminum substituting for silicon in tetrahedral coordination requires the coupled substitution of the alkalies to maintain local charge balance. The decrease in magma viscosity with increasing peralkalinity (Riebling 1966) indicates that alkalies in molecular excess of alumina are network modifiers and should, therefore, migrate to a less-polymerized melt. Thus the observed decrease with time in total mole percent alkalies at La Primavera is consistent with the implications of the two-liquid data. The less-polymerized melt presumably lies at a slightly deeper level of the magma chamber.

An additional piece of evidence for the role of melt structure in the post-caldera evolution of the Primavera magma chamber is the inverse correlation between whole-rock abundances and partition coefficients for the various REE. The percentage decrease in whole-rock abundance of a particular REE between the older and the younger ring domes is proportional to the percentage increase in that element's partition coefficient. LREE concentrations decrease greatly from the older ring domes to the youngest southern arc lava, whereas the HREE decrease only slightly (Figs. 5 and 6). As a result, the amount that a REE partition coefficient increases from the older to younger ring dome is a function of its ionic radius (Fig. 7a). The increase in partition coefficients is not simply a result of decreased concentrations in the glasses (which are approximately equal to whole-rock concentrations). REE were preferentially incorporated into the phenocrysts; their concentrations in sanidine, clinopyroxene, and fayalite actually increased even though bulk (and glass) concentrations declined. This is shown by a plot of the percentage increase of the partition coefficient for each REE versus its percentage decline in concentration in the glass (Fig. 7b); curves for all three analyzed phenocrysts lie above the line representing equal (but opposite) percentage changes in the partition coefficients and the REE concentrations in the glass phase.

Robinson (1974) has demonstrated that trivalent REE occupy dominantly octahedral sites within silicate melts, and Flynn and Burnham (1978) have suggested on the basis of vapor/melt partitioning experiments that these sites are smaller than 0.95 Å, the ionic radius of Yb. If this is the case, any decrease in the number of octahedral sites within the melt due to a decrease in either network-modifying cations or in the dissolved volatile content of the melt will be energetically unfavorable for all trivalent REE but HREE may be preferentially retained by the liquid relative to LREE because they are a better fit.

A complexing mechanism could also account for the greater change in LREE than HREE partition coefficients. Hydroxyl, fluoride, and phosphate all complex more strongly with HREE than LREE in aqueous solutions (Smith and Martell 1976). If this relationship holds in silicate melts, any decrease in concentration of these ligands may lead to a relatively larger increase in the activity of the LREE in the melt and to their preferential incorporation into phenocrysts.

Assuming that magma of any one eruptive group is derived from the uppermost portion of a magma chamber 150 $km^2$ in area, a layer of differentiated magma at least 20–50 m thick

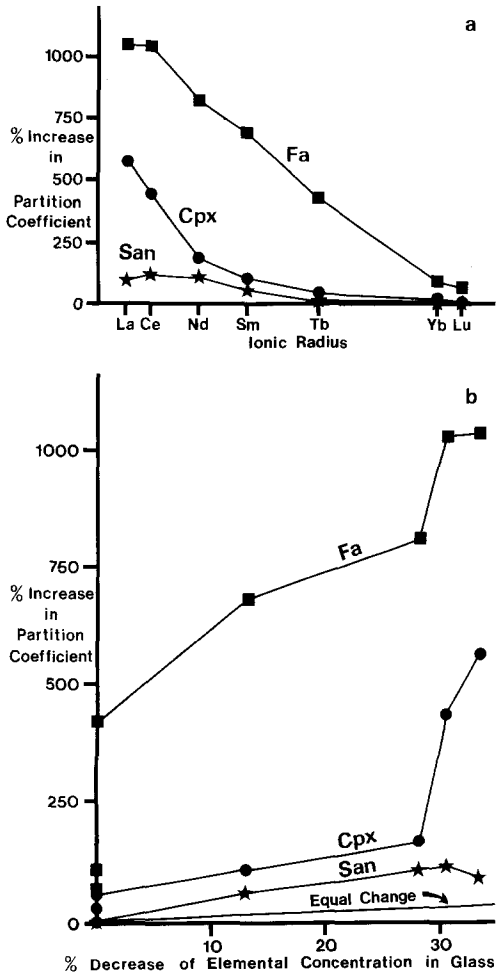


**Fig. 7a, b.** Correlation of change in partition coefficients with ionic radius and concentration in glass of the REE. **a** Percentage increase in partition coefficient from the 95,000- to the 75,000-year ring dome versus ionic radius. Partition coefficients for the LREE increase dramatically, while those for the HREE change little. **b** Percentage increase in the partition coefficient versus the percentage decrease in elemental concentration in the glass phase. All three phenocrysts plot above the line of equal (but opposite) change, showing that the REE were preferentially incorporated into the phenocrysts

is tapped by each group. Taking 20,000 years as the time between eruptive groups, diffusion through the total thickness would require diffusivities of 6 to $40 \times 10^{-6}$ $cm^2s^{-1}$. Diffusivities measured in *dry* rhyolitic glass range from $1 \times 10^{-6}$ $cm^2s^{-1}$ for Na to $5 \times 10^{-13}$ $cm^2s^{-1}$ for Eu at 800° C (Jambon and Carron 1973; Magaritz and Hofmann 1978). However, Watson (1979) found that the diffusivity of Cs in a *water-saturated* rhyolitic melt ($1 \times 10^{-8}$ $cm^2s^{-1}$) is 3.5 orders of magnitude greater than in dry glass, and Long (1978) calculated diffusivities for Sr and Ba in a vapor-saturated rhyolitic melt two orders of magnitude greater than those measured by Margaritz and Hoffmann (1978) in dry obsidian. Delaney and Karsten (1981) have recently confirmed Shaw's (1974) experimental work that demonstrated that the diffusivity of water in rhyolitic glasses increases with increasing water concentrations in the glass. If diffusivities of other elements are similarly increased in water-bearing melts, then diffusion may be a viable differentiation mechanism. Fifty meters, however, is probably still too far for an element to travel by diffusion alone in the 15,000- to 30,000-year repose periods between eruptions at La Primavera, even in water-rich melts. This constraint is lifted, however, if diffusion takes place across an interface between a static roof zone and a larger convecting volume below (Shaw et al. 1976), or if the compositionally-zoned chamber consists of many thin tabular convection cells so that mass transfer by diffusion need only occur at the boundaries between cells (Turner 1973, 1974, 1980; McBirney and Noyes 1979).

### *Phenocryst/Glass Partitioning in the Ash-Flow Magma and the Origin of Compositional Zoning in the Tala Tuff*

The last-erupted portion of the Tala Tuff (Sample 218) and its compositionally identical, outgassed equivalent, the south-central dome (Sample 317), are similar in major-element composition to the younger ring domes, and all three are lower in Ti, Fe, Mn, and Mg than the older ring dome. If bulk composition had been the major control on partition coefficients in the Tala Tuff magma, the last-erupted Tala Tuff, the south-central dome, and the younger ring dome could be expected to have similar partition coefficients, which, in turn, should be higher than those for the older ring dome. On the contrary, for the elements and phases analyzed, partition coefficients for most trace elements in the Tala Tuff magma (Table 9) are not only significantly smaller than in the younger ring domes, they are smaller than or similar to those in the more-mafic older ring dome.

Limited analytical data, thermodynamic calculations, and mineralogical evidence (Smith and Bailey 1966; Gibson 1970; Noble and Parker 1974; Sommer 1978; Hildreth 1977, 1979; R.L. Smith, personal communication, 1979; this study) indicate that first-erupted portions of ash-flow tuffs are enriched in $H_2O$, F, and Cl relative to the last-erupted portions, and, by inference, the roofward magmas are enriched in volatiles. Additional evidence for roofward enrichment in volatiles is the progressive increase in phenocryst content in the later-erupted portions of all ash-flow tuffs for which there are data. In the few cases for which Fe-Ti oxide temperatures are known (e.g., Bishop Tuff: Hildreth 1979; Paintbrush Tuff: Lipman 1971; Crater Lake: Ritchie 1980; Bandelier Tuff: R.L. Smith, personal communication 1979), this increase in phenocryst content is accompanied by an increase in magma temperature. For ash-flow tuffs with only slight major-element zonation, the progressive increase in phenocryst content with temperature demands that the parent magma chamber contain a gradient in dissolved volatiles; only a roofward increase in water and/or fluorine concentration could depress the temperatures of phase boundaries sufficiently to preclude crystallization in the cooler roof zone. Phase relations within the magma erupted from the Primavera magma chamber 95,000 years ago are consistent with this model and the conclusion that the magma chamber contained a volatile-enriched roof zone. The first-erupted part of the Tala Tuff is aphyric and the last-erupted portion contains less than 1% sanidine and quartz, whereas its outgassed continuation, the south-central dome, has, in addition, a trace of fayalite and ferrohedenbergite. The phenocryst content then increases to 10% in the north-central dome and older ring domes.

An increase in the water or halogen content of a melt, like an increase in concentration of the cationic network modifiers, should depolymerize the magma (Burnham 1975, 1979). One expression of such depolymerization could be *smaller* crystal/glass partition coefficients, as indeed are found in the Tala Tuff and its outgassed equivalent, the south-central dome. Additional evidence for the less-polymerized state of the ash-flow magma is the flatter phenocryst/glass partitioning patterns for REE in fayalite and ferrohedenbergite of the south-central dome and the

more-mafic older ring dome than for the compositionally similar younger ring dome (Mahood 1980a). Because the major-element compositions of ferrohedenbergite and fayalite do not change significantly (Tables 3 and 4), the flatter REE patterns at lower absolute values of the partition coefficients are consistent with there being a larger number of "octahedral sites" in the Tala Tuff magma and more-mafic older-ring-dome magma than in the younger-ring-dome magma. An increase in the number of octahedral sites decreases competition by the REE for those sites and thereby fails to promote preferential incorporation of LREE in the phenocrysts.

Enrichment of those elements (Si, Al, and the alkalies) which have been shown experimentally to partition into the more strongly polymerized melt would be antithetic to those elements (Fe, Ti, REE, Zr, Ta, etc.) that partition into the less polymerized melts if melt structure had been the dominant control on trace-element variations in the Tala Tuff. The vertical trace-element gradients in the Tala Tuff magma chamber are not consistent with such a model. Na and K behave antithetically, as do the HREE and LREE. Elements of the first transition series do not behave consistently: Sc and Ti are depleted and Zn is enriched roofward, while Fe is unzoned.

Additionally, if the distribution of elements in ash-flow magmas in general were controlled by melt structure alone, all the network-modifying elements would show the same direction of enrichment (which would be opposite that of the network-forming elements) in all systems. However, a number of elements that partition into less-polymerized melts in the two-liquid experiments have opposite enrichment directions in different ash-flow systems, despite the roofward depletion in all systems of Ca, Mg, and Ti. Zr, Hf, Zn, and Fe are enriched roofward in moderately to strongly peralkaline systems (e.g., Fantale Tuff: Gibson 1970; Grouse Canyon Member of the Belted Range Tuff: Noble and Parker 1974; Soldier Meadow Tuff: Korringa 1973), whereas these same elements are unzoned or depleted roofward in "calc-alkalic" systems (e.g., Bishop Tuff: Hildreth 1979; Topopah Springs Member of the Paintbrush Tuff: Lipman et al. 1966; Rainier Mesa Member of the Timber Mountain Tuff: Christiansen et al. 1977). In mildly peralkaline or alkali-rhyolite systems (e.g., La Primavera; Bandelier Tuff: Smith, personal communication 1979; Spearhead Member of the Thirsty Canyon Tuff: Noble and Parker 1974) these elements are variously unzoned or slightly enriched roofward.

The lack of coherent enrichment directions for chemically similar elements within the Tala Tuff magma-chamber and the different enrichment directions of elements such as Zr, Hf, Fe, and Zn in rhyolitic systems of slightly different bulk composition suggest that melt structure was not the dominant control on trace-element behavior in the Tala Tuff magma, presumably due to the depolymerizing effects of elevated volatile concentrations. Such behavior may be better explained by a mechanism in which trace elements migrate as volatile complexes in a thermal and gravitational gradient. Roofward enrichment in trace metals may be linked to roofward enrichment in the volatiles required to produce an ash-flow eruption. As volatiles move roofward, they may preferentially complex with different trace metals; thus, systems with different volatile contents or proportions of $H_2O$, F, Cl, and $CO_2$ will have different elemental enrichment patterns.

The differential transport of elements by an aqueous vapor phase in geologic materials within a thermal gradient has been demonstrated experimentally for only a few elements (e.g., K and Na: Orville 1963, and LREE and Y: Mineyev et al. 1966). Transport of trace elements as complexes in an *exsolved* vapor phase is unattractive as a dominant process in determining trace-element patterns in La Primavera magmas for two reasons: (1) There is little evidence that La Primavera magmas were saturated with respect to water prior to eruption. (2) If an exsolved vapor phase does not redissolve in the melt, the net effect will be transport of complexed trace metals out of the magma chamber and their depletion rather than enrichment in the uppermost magma *unless* (a) there is a sizable reservoir of the mobile trace elements in the deeper levels of the system, (b) vapor-melt partition coefficients decrease sharply with decreasing pressure and temperature, *and* (c) large volumes of metal-bearing vapor rise through the magma chamber and continuously exchange with the surrounding melt. In this way, the roofward portion of the magma chamber might become enriched in multivalent cations relative to lower levels.

The preferred model, however, is one in which *dissolved* trace-metal-volatile complexes migrate in a thermal and gravitational gradient. Such a model is speculative and not yet experimentally verified. Whether such complexes even exist within melts, let alone the senses and rates of their migration in thermal and gravitational gradients, is not known. Empirically, the data from ash-flow tuffs suggest that Zr, Hf, Fe, and Zn form stronger complexes with halogens than with water dissolved in silicic magmas, whereas the reverse is true of Sc. Elements that show the same direction of enrichment in both alkalic and calc-alkalic silicic systems (e.g., HREE) may form complexes of similar strength with both water and halogens. The low solubility of $CO_2$ in silicic melts (Holloway 1976) probably minimizes the role of dissolved carbonate complexes.

## Discussion and Conclusions

Gradients in temperature and phenocryst and whole-rock composition preserved in ash-flow tuffs are the main evidence for such gradients within silicic magma chambers and, inferentially, for melt structural gradients that may result from such zoning. The depolymerizing effect of roofward increase in concentration of dissolved volatiles is counteracted by the roofward decrease in temperature and concentration of network-modifying cations. Depending on the relative magnitudes of the individual gradients, the sum of their effects could result in maximum polymerization occurring at the roof, at deep levels, or at some intermediate position in a magma chamber.

In chambers in which the roof zone is strongly enriched in water or halogens, the melt may initially be increasingly polymerized with depth in the chamber, but as the water gradient flattens, increasing temperature and the more-mafic composition of the magma with increasing depth in the chamber may reverse the polymerization gradient. The result could be a magma chamber with a maximum in melt polymerization at some intermediate level. Transport of trace metals as dissolved volatile complexes may be the dominant differentiation mechanism in the volatile-rich zone above the polymerization maximum, while below the polymerization maximum (which would roughly coincide with the leveling of the water gradient), the distribution of trace metals may be determined by melt structure. This concept is shown diagramatically in Fig. 8a. An eruption that tapped through the polymerization maximum would sample magmas that obtained their trace-element abundance patterns through at least two different mechanisms; such an event might be manifest in discontinuities in elemental trends. This change in the dominant differentiation mechanism might account for apparent reversals in the trends of Zr, Hf, Na, and the agpaitic index between the Tala Tuff and older ring domes (although a transient

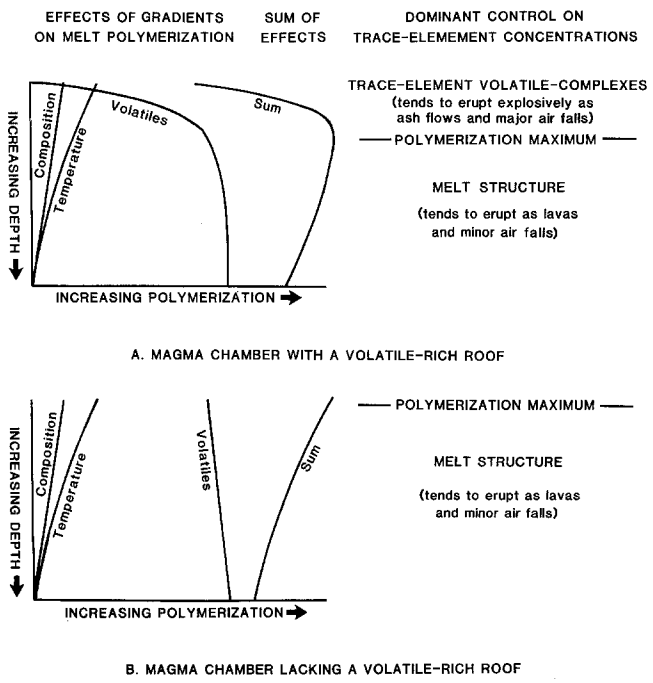


**Fig. 8a, b.** Diagrammatic representation of melt-polymerization gradients within silicic magma chambers. **a** Silicic magma chamber with a volatile-rich roof zone and maximum melt polymerization at an intermediate level. In the volatile-rich zone above the polymerization maximum, transport of trace metals as dissolved volatile complexes may be the dominant differentiation mechanism, while below the polymerization maximum, the distribution of trace metals may be determined by melt structure. **b** Silic magma chamber lacking a volatile-rich roof zone. The roofward magma might be the most polymerized, so most trace metals would diffuse to deeper, hotter, more-mafic levels of the chamber where the melt is less polymerized

vapor phase produced on eruption could have been involved). Magma that erupted as the south-central dome may have occupied the boundary between the two differentiation regimes. The reversals in a few trace-element trends and the agpaitic index coincide with the end of the ash-flow eruption, which is consistent with the idea that ash-flow eruptions cease on exhaustion of the volatile-enriched magma.

The roofward magma might be the most polymerized in a silicic magma chamber that lacks a strongly volatile-enriched roof zone. Thus most trace metals would diffuse to deeper, hotter, more-mafic levels of the chamber where the melt is less polymerized (Fig. 8b). Such a configuration might have produced the trends observed in the post-caldera lavas, each eruptive group representing successive samples of roof-zone magma in a relatively dry system that became progressively more silicic and more polymerized with time.

The upper portion of a magma chamber that contains melt structural gradients is either static or, if convecting, consists of many convection cells with small vertical dimensions. Migration of trace metals is facilitated in the latter case because diffusion is the rate-limiting step only at the interfaces between cells of contrasting melt structure, and the chemical gradients across these interfaces are constantly replenished by convection.

Two contrasting modes of liquid-state differentiation have been emphasized in the preceding discussion of the origin of the compositional zonation in the Tala Tuff and the chemical evolution of the post-caldera lavas: one involves transport of trace metals as volatile complexes within a thermal and gravitational gradient in a volatile-rich magma undersaturated with respect to water; the second involves emigration of trace elements in response to changes in melt structure produced by minor decreases in the concentration of cationic network modifiers, dissolved volatiles, and/or complexing agents in a relatively "dry" system. Both mechanisms could operate simultaneously and, at intermediate volatile concentrations, be of similar importance. Other differentiation mechanisms (e.g., crystal fractionation and contamination by assimilation of crustal material or by admixing of more mafic magmas from below) presumably influenced the compositions of magmas erupted at La Primavera, but their contribution has been largely obscured by the overprint of liquid-state differentiation mechanisms which operated in the high-level magma chamber.

It should be pointed out that the arguments presented here for melt structural control and volatile complexing in the differentiation of magmas can be strictly applied only to high-silica rhyolites and magmas rich in volatiles, respectively. The inadequacy of crystal settling and partial melting in explaining the zonation of the Tala Tuff magma chamber and the chemical trends with time in the post-caldera lavas does not bear upon the potential importance of these mechanisms in the differentiation of systems of other compositions. The composition of any derivative magma is determined by the relative efficiency of simultaneously operating differentiation mechanisms; for example, melt structural effects may dominate in highly polymerized high-silica rhyolites, but in low-viscosity andesites and basalts, crystal fractionation is more important. The relative efficiency of different mechanisms is controlled by physical properties of the melt (such as viscosity, density, and melt structure), the temperature gradient within the magma chamber, and the concentration of volatile components. Because convection aids diffusive transport, and because the nature of convection is determined by density as well as temperature gradients, the chemical evolution and rheological evolution of a silicic magma chamber are intertwined.

*Acknowledgements.* Lively discussions with E.W. Hildreth and I.S.E. Carmichael contributed to the ideas presented in this paper. Critical reviews of various drafts of this manuscript by Hildreth, C.M. Gilbert, Carmichael, W.P. Nash, and A. Ewart are greatly appreciated. J. Hampel, D. Kosco, and A. Grunder provided important technical support. I am grateful to R.L. Smith and R. Macdonald for arranging additional INAA and XRF analyses. Material support was provided by N.S.F. Grants EAR-74-12782 and EAR-78-03648 to Carmichael, and by two U.C. Berkeley Graduate Division Grants-in-Aid and a N.S.F. Fellowship to the author.

**Appendix 1.** Sample localities and descriptions[1]

| Sample number | Coordinates | Locality | Description |
|---|---|---|---|
| 15 | 2285.55, 659.95 | C. El Colli dome | Black obsidian with faint flow banding |
| 37 | 2292.15, 655.35 | A. La Cuartilla dome | Coarsely perlitic, friable, black vitrophyre |
| 40 | 2277.65, 661.35 | Eastern flow from the C. El Tajo center | Black obsidian with faint flow banding |
| 67 | 2276.30, 660.95 | Southeastern flow from the C. El Tajo center | Black obsidian with faint flow banding and sparse spherulites |
| 73 | 2275.85, 655.15 | A. Colorado dome | Dense black obsidian with sparse spherulites |
| 79 | 2281.50, 656.15 | A. Ixtahuatonte dome | Finely vesicular, grey, glassy, porphyritic rhyolite with slight iron staining around mafic phenocrysts |
| 83 | 2278.00, 647.35 | Llano Grande flow | Black obsidian with faint flow banding and sparse spherulites |
| 89 | 2290.75, 618.05 | M. El Burro dome | Coarsely perlitic, friable, black vitrophyre with slight iron staining around mafic phenocrysts |
| 90 | 2290.55, 618.15 | Cañon de Las Flores flow | Dense black obsidian |
| 92 | 2290.45, 649.55 | C. Chato dome | Coarsely perlitic, friable, black vitrophyre with slight iron staining around mafic phenocrysts |
| 105 | 2278.05, 646.10 | Western flow from the C. San Miguel center | Black obsidian with pumiceous streaks |
| 108 | 2281.60, 649.75 | La Puerta dome | Dull black obsidian |
| 115 | 2277.45, 651.50 | Southwestern flow from the C. Las Planillas center | Black obsidian with pumiceous streaks |
| 133 | 2281.50, 653.55 | C. El Tule dome | Coarsely perlitic, friable, black vitrophyre with pumiceous streaks and slight iron staining around mafic phenocrysts |
| 174 | 2283.50, 650.00 | Southeastern flow from the C. El Pedernal center | Light grey, finely vesicular, perlitic, porphyritic rhyolite with slight iron staining around mafic phenocrysts |
| 175 | 2284.50, 648.80 | Northwestern flow from the C. El Pedernal center | Black obsidian with grey pumiceous streaks |
| 184 | 2280.40, 641.10 | Near A. El Taray, west of C. San Miguel | White, aphyric, pumice lapilli from the first member of the Tala Tuff |
| 186 | 2288.65, 646.75 | M. El León dome | Light grey, pumiceous, porphyritic rhyolite with slight iron staining around mafic phenocrysts |
| 193 | 2287.70, 647.55 | Río Salado dome | Grey, pumiceous, porphyritic rhyolite with slight iron staining around mafic phenocrysts |
| 210 | 2287.90, 648.60 | A. El Gallo near its mouth, east of Río Caliente | White, aphyric, pumice lapilli from the upper portion of the first member of the Tala Tuff |
| 218 | 2287.90, 650.40 | Cliff on south side of A. Arena Grande | White, sparsely porphyritic, pumice lapilli from the third member of the Tala Tuff |
| 234 | 2289.15, 661.85 | Tributary to A. Arena Chica | White, sparsely porphyritic, pumice lapilli from the giant pumice horizon |
| 252 | 2285.85, 650.50 | A. El Gallo, east of C. El Pedernal | Dark grey, sparsely porphyritic, pumice lapilli from the second member of the Tala Tuff |
| 255 | 2289.75, 663.45 | Arroyo south of A. Milpa Alta, 1 km NW of Univ. Agric. de Guadalajara | White, aphyric, pumice lapilli from the first member of the Tala Tuff |
| 256 | 2289.15, 661.85 | Arroyo south of A. Milpa Alta, just east of railroad tracks | White, aphyric, pumice lapilli from the first member of the Tala Tuff |
| 283 | 2288.30, 651.00 | Lower part of C. Alto | Coarsely perlitic, friable, black vitrophyre |
| 290 | 2272.50, 652.55 | A. Saucillo group, north of A. Saucillo | Dense black obsidian |
| 317 | 2282.10, 653.20 | Lower part of M. El Nejahuete | Dense, black, sparsely porphyritic vitrophyre |

1 The abbreviations A., C., and M. stand for arroyo, cerro (hill), and mesa, respectively. All sample localities are found on Detenal map sheet Guadalajara Oeste F-13-D-54

## References


Arth JG (1976) Behavior of trace elements during magmatic processes – A summary of theoretical models and their applications. J Res US Geol Surv 4:41–47

Bailey RA, Dalrymple B, Lanphere MA (1976) Volcanism, structure, and geochronology of Long Valley caldera, Mono Country, California. J Geophys Res 81:725–744

Billings MP (1956) The geology of New Hampshire, Part II, Bedrock Geology. Concord: New Hampshire State Planning Commission

Buddington AF, Lindsley DH (1964) Iron-titanium oxide minerals and synthetic equivalents. J Petrol 5:310–357

Burnham CW (1975) Thermodynamics of melting in experimental silicate-volatile systems. Fortschr Mineral 52:101–118

Burnham CW (1979) Magmas and hydrothermal fluids. In: HL Barnes (ed) Geochemistry of hydrothermal ore deposits, pp 71–136. New York, John Wiley and Sons

Byers FM Jr, Carr WJ, Orkild PP, Quinlivan WD, Sargent KA (1976) Volcanic suites and related cauldrons of Timber Mountain – Oasis Valley caldera complex, southern Nevada. US Geol Surv Prof Pap 919:1–70

Carmichael ISE (1967) The iron-titanium oxides of salic volcanic rocks and their associated ferromagnesian silicates. Contrib Mineral Petrol 14:36–64

Carmichael ISE, Hampel J, Jack RN (1968) Analytical data on USGS Standard Rocks. Chem Geol 3:59–64

Christiansen RL, Noble DC (1965) Black Mountain volcanism of southern Nevada. Abstr for 1964. Geol Soc Am Spec Pap 82:246

Christiansen RL, Lipman PW, Carr WJ, Byers FM Jr, Orkild PP, Sargent KA (1977) Timber Mountain-Oasis Valley caldera complex of southern Nevada. Geol Soc Am Bull 88:943–959

Delaney JR, Karsten JL (1981) Ion microprobe studies of water in silicate melts: concentration-dependent water diffusion in obsidian. Earth Planet Sci Lett 52:191–202

Flynn RT, Burnham CW (1978) An experimental determination of rare earth partition coefficients between a chloride containing vapor phase and silicate melts. Geochim Cosmochim Acta 42:685–701

Gibson IL (1970) A Pantelleritic Welded Ash-Flow Tuff from the Ethiopian Rift Valley. Contrib Mineral Petrol 28:89–111

Ghiorso MS, Carmichael ISE (1980) A regular solution model for meta-aluminous silicate liquids: Applications to geothermometry, immiscibility, and the source regions of basic magmas. Contrib Mineral Petrol 71:323–342

Häkli TA, Wright TL (1967) The fractionation of nickel between olivine and augite as a geothermometer. Geochim Cosmochim Acta 31:877–884

Hart SR, Davis K (1978) Nickel partitioning between olivine and silicate melt. Earth Planet Sci Lett 40:203–219

Hildreth EW (1977) The magma chamber of the Bishop Tuff: Gradients in temperature, pressure, and composition. University of California, Berkeley, Unpubl Ph D dissert, 328 p

Hildreth W (1979) The Bishop Tuff: Evidence for the origin of compositional zoning in silicic magma chambers. Geol Soc Am Spec Pap 180:43–75

Hildreth W, Christiansen RL, O'Neil JR (1980) Catastrophic isotopic modification of rhyolitic magma by creation of the Yellowstone caldera. Geol Soc Am, Abstr with Progr 12:111

Holloway JR (1976) Fluids in the evolution of granitic magmas: Consequences of finite $CO_2$ solubility. Geol Soc Am Bull 87:1513–1518

Jacobsen RRE, MacLeod WN, Black R (1958) Ring complexes in the Younger Granite Province of northern Nigeria. Geol Soc London Mem 1

Jambon A, Carron J-P (1973) Etude expérimentale de la diffusion des éléments alcalins K, Rb, Cs dans une obsidienne granitique. CR Acad Sci Paris 276:3069–3072

Korringa MK (1973) Linear vent area of the soldier meadow tuff, an ash-flow sheet in Northwestern Nevada. Geol Soc Am Bull 84:3849–3866

Lipman PW (1971) Iron-titanium oxide phenocrysts in compositionally zoned ash-flow sheets from Southern Nevada. J Geol 79:438–456

Lipman PW, Christiansen RL, O'Connor JT (1966) A compositionally zoned ash-flow sheet in southern Nevada. US Geol Surv Prof Pap 524-F; 1–47

Long PE (1978) Experimental determination of partition coefficients for Rb, Sr, and Ba between alkali feldspar and silicate liquid. Geochim Cosmochim Acta 42:833–846

Maaløe S, Wyllie PJ (1975) Water content of a granite magma deduced from the sequence of crystallization determined experimentally with water-undersaturated conditions. Contrib Mineral Petrol 52:175–191

Macdonald R, Bailey DK (1973) Data of geochemistry, Chapter N. Chemistry of igneous rocks, Part 1. The Chemistry of the peralkaline oversaturated obsidians. US Geol Surv Prof Pap 440-N-1:1–37

Magaritz M, Hofmann AW (1978) Diffusion of Eu and Gd in Basalt and Obsidian. Geochim Cosmochim Acta 42:847–858

Mahood GA (1980a) The geological and chemical evolution of a late pleistocene rhyolitic center: The Sierra La Primavera, Jalisco, Mexico. University of California, Berkeley, Unpublished Ph D dissert, 245 p

Mahood GA (1980b) Geological evolution of a Pleistocene rhyolitic center – Sierra La Primavera, Jalisco, México. J Volcanol Geotherm Res 8:199–230

Mahood G, Hildreth W Large trace-element partition coefficients in high-silica rhyolites (in preparation)

McBirney AR, Noyes RM (1979) Crystallization and layering of the Skaergaard intrusion. J Petrol 20:487–554

Mineyev DA, Dikov Yu P, Sobolev BP, Borutskaya VL (1966) Differentiation of rare-earth elements under supercritical conditions. Geochem Int 3:357–359

Mysen BO, Virgo D (1980) Trace element partitioning and melt structure: an experimental study at 1 atm pressure. Geochim Cosmochim Acta 44:1917–1930

Mysen BO, Virgo D, Scarfe CM (1980) Relations between the anionic structure and viscosity of silicate melts: a Raman spectroscopic study at 1 atmosphere and at high pressure. Am Mineral 65:690–711

Naney MT, Swanson SE (1980) The effect of Fe and Mg on crystallization in granitic systems. Am Mineral 65:639–653

Nicholls J, Carmichael ISE, Stormer JC (1971) Silica activity and $P_{total}$ in igneous rocks. Contrib Mineral Petrol 33:1–20

Noble DC (1968) Kane Springs Wash Volcanic Center, Lincoln Country, Nevada. Geol Soc Am Mem 110:109–116

Noble DC, Parker DF (1974) Peralkaline silicic volcanic rocks of the Western United States. Bull Volcanol 38:803–827

Noble DC, Haffty J, Hedge CE (1969) Strontium and magnesium contents of some natural peralkaline silicic glasses and their petrogenetic significance. Am J Sci 267:598–608

Noble DC, Sargent KA, Mehnert HH, Ekren EB, Byers FM Jr (1968) Silent Canyon volcanic center, Nye County, Nevada. Geol Soc Am Mem 110:65–76

Orville PM (1963) Alkali ion exchange between vapor and feldspar phases. Am J Sci 261:201–237

Riebling EF (1966) Structure of sodium aluminosilicate melts containing at least 50 mole % $SiO_2$ at 1,500° C. J Chem Physics 44:2857–2865

Ritchie JL (1980) Divergent magmas at Crater Lake, Oregon: Products of fractional crystallization and vertical zoning in a shallow, water-undersaturated chamber. J Volcanol Geotherm Res 7:373–386

Robinson CC (1974) multiple sites for $Er^{3+}$ in alkali silicate glasses (I). The principal sixfold coordinated sites of $Er^{3+}$ in silicate glass. J Non-Cryst Solids 15:1–10

Ryerson FJ, Hess PC (1978) Implications of liquid-liquid distribution coefficients to mineral-liquid partitioning. Geochim Cosmochim Acta 42:921–932

Schnetzler CC, Philpotts JA (1970) Partition coefficients of rare-earth elements between igneous matrix material and rock-forming mineral phenocrysts-II. Geochim Cosmochim Acta 34:331–340

Shaw HR (1974) Diffusion of water in granitic liquids, I. Experimental data. II. Mass transfer in magma chambers. In: AW Hofmann, BJ Giletti, HS Yoder Jr, RA Yund (eds) Geochemical transport kinetics. Carnegie Inst Washington Publ 634:139–170

Shaw HR, Smith RL, Hildreth W (1976) Thermogravitational mechanisms for chemical variations in zoned magma chambers. Geol Soc Am, Abstr With Progr 8:1102

Smith RL (1979) Ash-flow magmatism. Geol Soc Am Spec Pap 180:5–27

Smith RL, Bailey RA (1966) The Bandelier Tuff: A study of ash-flow eruption cycles from zoned magma chambers. Bull Volcanol 29:83–104

Smith RL, Macdonald R (1979) Rhyolitic volcanism and its relationship to granitic plutonism. Geol Soc Am Abstr with Progr 11:520

Smith RM, Martell AE (1976) Critical stability constants, Vol 4: Inorganic Complexes. New York-London, Plenum Press

Sommer II MA (1978) Volatiles in silicate melt inclusions from the air-fall and ash-flow tuffs of the Bandelier Tuff, Jemez Mountains, New Mexico. Geol Soc Am, Abstr with Progr 10:495

Takahashi E (1978) Partitioning of $Ni^{2+}$, $Co^{2+}$, $Fe^{2+}$, $Mn^{2+}$, and $Mg^{2+}$ between olivine and silicate melts: compositional dependence of partition coefficients. Geochim Cosmochim Acta 42:1829–1844

Turner JS (1973) Buoyancy effects in fluids. London, Cambridge Univ Press

Turner JS (1974) Double-diffusive phenomena. Annu Rev Fluid Mech 6:37–56

Turner JS (1980) A fluid dynamical model of differentiation and layering in magma chambers. Nature 285:213–215

Virgo D, Mysen BO, Kushiro I (1980) Anionic constitution of silicate melts quenched at 1 atm from Raman spectroscopy: Implications for the structure of igneous melts. Science 208:1371–1373

Watson EB (1976) Two-liquid partition coefficients: Experimental data and geochemical implications. Contrib Mineral Petrol 61:35–48

Watson EB (1977) Partitioning of manganese between forsterite and silicate liquid. Geochim Cosmochim Acta 41:1363–1374

Watson EB (1979) Diffusion of cesium ions in $H_2O$-saturated granitic melt. Science 205:1259–1260

Watson EB (1979) Zircon saturation in felsic liquids: Experimental results and applications to trace element geochemistry. Contrib Mineral Petrol 70:407–420

Wones DR, Eugster HP (1965) Stability of biotite: experiment, theory and application. Am Mineral 50:1228–1272

Wright TL, Doherty PC (1970) A linear programming and least squares computer method for solving petrologic mixing problems. Geol Soc Am Bull 81:1995–2008

Wyllie PJ, Tuttle DF (1961) Experimental investigations of silicate systems containing two volatile components, II. The effects of $NH_3$ and HF, in addition to $H_2O$, on the melting temperatures of albite and granite. Am J Sci 259:128–143

Received November 13, 1980; Accepted April 1, 1981